

Magnon Hall effect in antiferromagnetic lattices

P. G. de Oliveira^{a*}

E-mail address: pgopedro@ufmg.br

and

A. S. T. Pires^a

E-mail address: antpires@fisica.ufmg.br

^a Departamento de Física, Universidade Federal de Minas Gerais, Belo Horizonte, MG, CP702, 30123-970, Brazil.

* Corresponding author.

Abstract

Topology applied to condensed matter is an important area of research and technology, and topological magnetic excitations have recently become an active field of study. This paper presents a general discussion of magnon Hall transport in two-dimensional antiferromagnets. Although the Chern number is zero for a collinear antiferromagnet, we offer a general discussion that can be used in the more general case. First, we study the Union Jack lattice, where an effective time-reversal symmetry is broken, making the system display the magnon Hall effect. Then, we investigate the brick-wall lattice where such symmetry is present. Consequently, we have a phenomenon similar to the quantum spin Hall effect in electronic systems. Both lattices have not yet been studied from the topological point of view. The coexistence of opposite spin polarization in an antiferromagnet resembles the electron spin in various transport phenomena. We study magnon transport in the lattices mentioned above with Dzyaloshinskii-Moriya interaction and easy-axis single-ion anisotropy. We calculate the Berry curvature from the eigenvalues of the Hamiltonian. From that, we plot the spin Hall and thermal Hall conductivities, as well as the spin Nernst coefficient, as functions of the temperature. In the Union Jack lattice, we treat the effect of anharmonic interactions using a mean-field spin wave theory where the Hamiltonian becomes implicitly temperature-dependent. We determine self-consistently the renormalized dispersion and the staggered magnetization as a function of temperature. Our calculations can be applied to other antiferromagnetic lattices.

Keywords: topological magnons, spin Nernst effect, thermal Hall effect, magnon transport

1 Introduction

Over the past decades, topology has played an essential role in condensed matter physics, and one of the most studied phenomena is the quantum Hall effect (QHE). Suppose we have electrons localized in the xy -plane subjected to a magnetic field pointing in the up z -direction. We consider also a current I_x along the x -direction, associated with a current density j_x and an electric field E_x . The transversal magnetic field deflects the electrons sideways in the negative y -direction. If the sample is infinite in the y -direction, the electrons will move with some angle relative to the x -axis. But if the sample is finite in the y -direction, the deflected electrons will accumulate on the edge of the sample, and will produce a transversal electric field E_y . In a sample with a strip geometry, the QHE makes electrons at the top edge flow to the right while electrons at the bottom move to the left. We have $J_\alpha = \sigma_{\alpha\beta} E_\beta$. The time-reversal (TR) operation inverts J_α but not E_β . Therefore, $\sigma_{\alpha\beta}$ must break time-reversal symmetry (TRS). This Hall current is dissipationless, contrary to a longitudinal current, which breaks TRS through energy dissipation. In the QHE, the TRS is broken by an external magnetic field [1] or internal magnetic fluxes, like in the Haldane model [2]. The QHE states, also called Chern insulators, are characterized by a non-zero Chern number, which indexes the topological phases of the system.

Chern insulators only exist in two dimensions and rely on time-reversal symmetry breaking. However, another topological class can be present even when TRS is preserved. In the so-called quantum spin Hall effect (QSHE) [3], time-reversal symmetry is preserved due to the absence of external magnetic fields. Spin-orbit coupling generates an effective magnetic field that acts upward on the spin-up and downward on the spin-down electrons. As a result, electrons with opposite spins move in opposite directions (in separate conducting channels) at the edges of the sample. There is no net flow of charge, only a net spin current. In the QSHE, the spin current is even under the TRS, so $\sigma_{xy} \neq 0$ is consistent with this symmetry. In the top edge of a sample with a strip geometry, spin-up electrons move in one direction (say, right), spin-down electrons move in the opposite direction (left), and vice-versa at the bottom edge. Systems supporting the QSHE have null a Chern number but can be indexed by a two-valued topological integer. They are often called \mathbb{Z}_2 topological insulators. The edge currents are protected by time-reversal symmetry. Generally, if an electron backscatters, its spin is flipped, and time reversal symmetry is broken. But there will be no backscattering if TRS is present (as it happens when there is a non-magnetic impurity). Time-reversal symmetry is always present in \mathbb{Z}_2 topological insulators, so the edge modes are robust against backscattering. Topological systems have a topologically nontrivial band structure. Its bulk is insulating, and its surface/edge is a topologically protected conductor [4, 5].

We can find topological states not only in electronic systems but also in ordered magnetic lattices, where quantized perturbations in the magnetic order, the so-called magnons, are the spin carriers. Topological two-dimensional magnets display a finite magnon Hall conductivity that can be used in magnonic nanodevices. They can also show topologically protected edge modes, which are robust against structural or magnetic disorder and can form ideal waveguides for long-range magnon transport [6]. An essential property of noninteracting topological magnons is that they can propagate for a long time without dissipation. They do not interact strongly with other degrees of freedom and are, for this reason, adequate to be used in spintronics. The quantum Hall effect requires high magnetic fields, which limits its use in technology applications, whereas magnon transport does not require an external magnetic field. Note that in the QSHE, spins are carried out by the electrons. In magnets, the spin of the atoms is fixed, and what is carried out is the spin of the magnons (non-localized excitations): we have a magnonic spin current. Magnons can mediate various Hall-like transport phenomena in both ferromagnets (FM) and antiferromagnets (AF). For example, a transverse spin current appears in response to a magnetic field gradient (which plays the role of an electric field in electronic systems), or a transverse heat current, mediated by magnons, manifests in response to a thermal gradient. The spin Nernst effect is a spin current caused by a temperature gradient. The Nernst-Ettinghausen effect is a heat current in response to a magnetic field gradient [7].

We should remark that electron and magnon systems are quite different. In the case of electrons, the energy levels are filled at zero temperature up to the Fermi energy (so we can have transport at zero temperature). We have conduction and valence bands, and conductors and insulators have different properties. For magnons, there is no Fermi energy. We have zero magnons at zero temperature and, therefore, no transport. We can have transitions from a filled band to another one since the Pauli exclusion principle does not apply here. Another difference from fermionic systems is that we can have a magnon spin Hall effect (spin current in response to a magnetic field gradient) even when the Chern number is zero. A topological ferromagnet (or antiferromagnet) is usually called a topological magnon insulator, although the term “insulator” has no physical meaning for magnons. Here, we generically call magnon Hall effect the transverse current originated by a longitudinal field gradient. The effect can be topological when the Chern number differs from zero or geometrical when it vanishes.

As shown by Liu et al. [8], Chern numbers in collinear antiferromagnets are expected to be zero. Some special in-plane magnetic configuration is required for a non-null Chern number. Yet, it is possible to have topologically protected edge modes even when the Chern number is zero due to an effective time-reversal symmetry. That is the case of the pure spin Nernst effect in the brick-wall lattice studied in this paper.

Transport phenomena in magnetic systems are essential tools for studying magnetic excitations and fluctuations. These techniques have become available as a probe due to the development of experimental methods in the context of spintronics, and in the last decades, there has been a great interest in studying topological effects in spin models [7-91]. Antiferromagnets exhibit ultrafast dynamics and are robust against reasonably large external fields. They are a competitive alternative to ferromagnets to store and manipulate information [10], as topological ferromagnets present drawbacks such as strong magnetic disturbances and low mobility due to high magnetization. Topological transport in AF magnets is a developing field and has been investigated in several contexts: collinear paramagnets [11], non-collinear and non-coplanar magnets [12-14], and dimmer systems [15-17]. Also, topological transport relies on a system's property called Berry curvature, which can be induced and controlled by several mechanisms, like electromagnetic waves [18] or crystal chirality [19]. Topological magnonics is a fast-evolving field. In this scenario, it is essential to study antiferromagnetic topological insulators in all kinds of lattices and compare their thermomagnetic properties.

This paper is organized as follows. In Section 2, we give a brief introduction to the magnon Hall effect following Ref. [7]. In Section 3, we study the transport of spins starting from the Kubo formula and show how to relate the Hall conductivity to the Berry curvature. Section 4 presents a generalized Bogoliubov transformation to diagonalize the Hamiltonian of antiferromagnets. The Union Jack lattice is introduced in Section 5. In Section 6, we present a brief discussion of symmetries. In Section 7, the transport coefficients are introduced. The brick-wall lattice is investigated in Section 8. In Section 9, we summarize our results. Finally, in Appendix A, we treat the contribution of four operator terms using a self-consistent mean-field spin wave theory, and in Appendix B, we derive an expression for the Berry curvature from the eigenvalues of a general antiferromagnetic Hamiltonian.

2 Magnon Hall effect

As discussed in the following, one can make a reasonable (but not entirely equivalent) correspondence between the electronic spin degrees of freedom in a topological insulator with the two sublattice degrees of freedom in an antiferromagnet. In an analogy to TIs, we can study the topological properties of antiferromagnets and establish a bosonic version of the QSHE where the spin carriers are not electrons but magnons. In this section, we follow Ref. [7] and give a qualitative description of what happens in some topological antiferromagnets.

Based on the symmetry of Maxwell's equations, Aharonov and Casher [92] considered the interaction between a particle's magnetic dipole moment and an electric field and introduced a dual to the Aharonov-Bohm effect, as we show in the following.

Suppose a two-dimensional ferromagnet in the xy -plane is subjected to a spatially varying electric field $\mathbf{E}(\mathbf{r})$. Through the Aharonov-Casher effect, $\mathbf{E}(\mathbf{r})$ couples to magnons' magnetic dipole moment $g\mu_B\hat{\mathbf{z}}$. A moving magnetic dipole interacts with the external electric field and acquires an Aharonov-Casher phase due to hopping between the sites given by

$$\theta_{ij} = \frac{g\mu_B}{\hbar c^2} \int_{x_i}^{x_j} d\mathbf{r} \cdot (\mathbf{E}(\mathbf{r}) \times \hat{\mathbf{z}}). \quad (1)$$

The exchange Hamiltonian in the presence of the AC effect can be written as [7,9]:

$$H = - \sum_{\langle i,j \rangle} \frac{J_{ij}}{2} [(S_i^+ S_j^- e^{i\theta_{ij}} + S_i^- S_j^+ e^{-i\theta_{ij}}) + S_i^z S_j^z] \quad (2)$$

where θ_{ij} is the AC phase the magnetic dipole moment, associated with the spin along the z -direction, acquires when it hops between neighboring sites x_i and x_j .

The Hamiltonian of a ferromagnet with Dzyaloshinskii-Moriya (DM) interaction with the DM vector given by $\mathbf{D}_{ij} = \pm D\hat{\mathbf{z}}$ can be written as an expression analogous to Eq. (2), even without the presence of an electric field $\mathbf{E}(\mathbf{r})$ [34], as we show in the following.

A Hamiltonian with FM exchange and Dzyaloshinskii-Moriya interaction between near-neighbor sites is written as:

$$\begin{aligned}
H &= -J \sum_{\langle i,j \rangle} \mathbf{S}_i \cdot \mathbf{S}_j + \sum_{\langle i,j \rangle} \mathbf{D} \cdot \mathbf{S}_i \times \mathbf{S}_j \\
&= -J \sum_{\langle i,j \rangle} \mathbf{S}_i \cdot \mathbf{S}_j \pm D \sum_{\langle i,j \rangle} \hat{\mathbf{z}} \cdot \mathbf{S}_i \times \mathbf{S}_j
\end{aligned} \tag{3}$$

Using the ladder operators, we can develop this as:

$$\begin{aligned}
H &= -J \sum_{\langle i,j \rangle} (S_i^x S_j^x + S_i^y S_j^y + S_i^z S_j^z) \pm D \sum_{\langle i,j \rangle} (S_i^x S_j^y - S_i^y S_j^x) \\
&= -\frac{J}{2} \sum_{\langle i,j \rangle} (S_i^+ S_j^- + S_i^- S_j^+) \pm \frac{iD}{2} \sum_{\langle i,j \rangle} (S_i^+ S_j^- - S_i^- S_j^+) + J \sum_{\langle i,j \rangle} S_i^z S_j^z \\
&= -\sum_{\langle i,j \rangle} \left(\frac{J \mp iD}{2} S_i^+ S_j^- + \frac{J \pm iD}{2} S_i^- S_j^+ \right) + J \sum_{\langle i,j \rangle} S_i^z S_j^z
\end{aligned} \tag{4}$$

We can define a phase $\theta = \tan^{-1}(D/J)$, so we have:

$$\sin \theta = \frac{D}{\sqrt{J^2 + D^2}}, \quad \cos \theta = \frac{J}{\sqrt{J^2 + D^2}} \tag{5}$$

Also note that $J \pm iD = \sqrt{J^2 + D^2} e^{\pm i\theta}$. Hence, The Hamiltonian can be written as

$$H = -\frac{\tilde{J}}{2} \sum_{\langle i,j \rangle} (e^{\mp i\theta} S_i^+ S_j^- + e^{\pm i\theta} S_i^- S_j^+) + J \sum_{\langle i,j \rangle} S_i^z S_j^z \tag{6}$$

with $\tilde{J} = \sqrt{J^2 + D^2}$. That has the same form as Eq. (2), showing that the DM vector \mathbf{D} plays the role of a vector potential for magnons, and an external electric field is not necessary to induce the effects to be described below. However, for simplicity, we will consider that the source of the AC effect is a (spatially varying) static electric field, as it is usually done when presenting this subject. For an isotropic antiferromagnet (for instance, in a square lattice) with spin-rotational symmetry around the z-axis and in the linear spin wave approximation, up and down magnons are completely decoupled, and the dynamics of magnons is described as the combination of two independent copies of the dynamics of magnons in a ferromagnet for each mode [4,5]. To proceed with the discussion, we will consider a Hamiltonian with degenerate up and down magnons.

In the absence of the AC term, a magnetic field gradient $\partial_x B$ along the x-axis gives origin to a force $F_\sigma = \sigma g \mu_B \partial_x B$, where $\sigma = -1$ for the ferromagnet and $\sigma = \pm 1$ for the antiferromagnet. That drives antiferromagnetic magnons in the bulk with opposite magnetic moments to flow in opposite $\pm \hat{\mathbf{x}}$ directions (since the directions of the forces are opposite for the two magnons modes), generating a longitudinal spin current without a net heat current. On the other hand, when subjected only to a thermal gradient $\partial_x T$, both spin-up and spin-down magnons flow in the same direction. The spin current vanishes, but there is a net longitudinal heat current. That is the conventional transport behavior of an antiferromagnetic magnonic system (see first column of Table 1).

To study transversal (Hall) transport in antiferromagnets, we analyze magnons in an electric field $\mathbf{E}(\mathbf{r})$. We must replace the momentum operator \mathbf{p} by $\mathbf{p} + \sigma g \mu_B \mathbf{A}/c$, where [92]:

$$\mathbf{A}(\mathbf{r}) = \frac{1}{c} \mathbf{E}(\mathbf{r}) \times \hat{\mathbf{z}} \tag{7}$$

Hence, the Hamiltonian in the low-energy dynamics and in the continuum approximation (that is, the Hamiltonian of a gas of noninteracting magnons) is given by $H = \sum_{\sigma=\pm} H_\sigma$, with:

$$H_\sigma = \frac{1}{2m} \left(\mathbf{p} + \frac{\sigma g \mu_B}{c} \mathbf{A} \right)^2 - \sigma g \mu_B B \tag{8}$$

where m is the effective magnon mass. We can see that the Hamiltonian above is formally identical to the one from a charged particle on a magnetic field, with \mathbf{A} playing the role of the vector potential and $\sigma g \mu_B$ being the coupling constant (instead of e).

If the spatially varying static electric field has the form $\mathbf{E}(\mathbf{r}) = E(-x/2, -y/2, 0)$, where E is a constant, from Eq. (7) we obtain a gauge potential $\mathbf{A}(\mathbf{r}) = (E/c)(-y/2, +x/2, 0)$, which gives :

$$\nabla \times \mathbf{A} = \frac{E}{c} \hat{\mathbf{z}}, \quad (9)$$

and we can see that E plays the role that, in charged particles, is played by magnetic fields. From the canonical equation of motion, we find that the force acting on magnons is

$$\mathbf{F}_{AC} = \sigma g \mu_B \left[\nabla B - \frac{\mathbf{v}}{c} \times (\nabla \times \mathbf{A}) \right]. \quad (10)$$

Using (9), we can write

$$\mathbf{F}_{AC} = \sigma g \mu_B \left[\nabla B - \frac{\mathbf{v}}{c^2} \times E \hat{\mathbf{z}} \right], \quad (11)$$

and again, comparing \mathbf{F}_{AC} to the Lorentz force in charged particles ($\mathbf{F}_e = e[\mathbf{E} + \mathbf{v} \times \mathbf{B}]$), we note the parallel between electronic and magnonic transport in the presence of EM fields: the roles that electric and magnetic fields have in electronic systems is played, respectively, by ∇B and $-E\hat{\mathbf{z}}/c^2$ in magnonic systems.

The velocity \mathbf{v} is constituted of two parts: the cyclotron velocity \mathbf{v}_c and the drift velocity \mathbf{v}_d . The drift velocity is the velocity of the guiding center, meaning that in the drifting frame, the velocity comes only from the cyclotron motion. Supposing that $\frac{d}{dt}\mathbf{v}_d = 0$, we find $\mathbf{v}_d \times \hat{\mathbf{z}} = (c^2/E) \nabla B$ [7]. If the magnetic field gradient is applied along the x-axis ($\nabla B = \partial_x B \hat{\mathbf{x}}$), we get $\mathbf{v}_d = (0, (c^2/E) \partial_x B, 0)$, which is independent of σ and perpendicular to $\partial_x B \hat{\mathbf{x}}$. Thus, all magnons (with spin up and down) flow in the same $\hat{\mathbf{y}}$ direction when subjected to electric and magnetic field gradients. The transversal spin current vanishes in the bulk, while the heat current is nonzero. On the other hand, a thermal gradient generates helical magnon Hall transport in the bulk where up and down magnons flow in opposite directions. Since magnons of up and down spins convey down and up spins, respectively, a nonzero spin current appears while the total heat current cancels out (see the second column of Table 1). A more detailed discussion about the thermomagnetic properties can be done using Onsager coefficients, which relate thermal and magnetic field gradients with current and heat densities in the bulk [93].

That qualitatively describes the Hall transport of magnons in the bulk of an AF magnet, which is generated by coupling magnons with a static and spatially varying electric field through the Aharonov-Casher effect. The thermomagnetic properties of AF magnets are summarized in Table 1. We stress that these conclusions were made in the assumption that we are in the linear response regime, where sufficiently low temperature and applied magnetic fields make the energy bands almost degenerate. If the band degeneracy is lifted, as in the case of the Union Jack lattice studied in Section 5, both spin and heat Hall currents can be simultaneously different from zero.

Even though the formalism above requires static electric fields or DM vectors, it is known that the same result can be achieved with an oscillating electromagnetic field [18]. That has the advantage that electromagnetic waves can be easily tuned. The Floquet theory enables one to transform a time-dependent model into an effective static model governed by the so-called Floquet Hamiltonian. As a result, we get a synthetic tunable intrinsic DMI in quantum magnets without an inversion center. This can be achieved with the application of a circularly polarized laser with a dominant oscillating electric field component perpendicular to the magnetic 2D material. Another advantage of oscillating fields is that they amplify topological magnons via dipolar coupling [94, 95]. This interaction contributes to the complex off-diagonal term f_k of a magnon Hamiltonian (See Eq. (63)), which is related to the Berry curvature. That term is associated with the DMI in the Union Jack lattice, while in the brick-wall lattice it is associated with a complex structure factor. The interaction with an oscillating electric field can amplify these terms and enhance transverse transport.

Regarding the edge properties of the system, we see from the discussion under Eq. (11) that the static drift velocity $\mathbf{v}_d = (0, (c^2/E) \partial_x B, 0)$ vanishes in the bulk if the magnetic field gradient is zero. However, each magnon still performs a cyclotron motion in opposite directions due to the static electric field $\mathbf{E}(\mathbf{r})$. So in the presence of a thermal gradient, we have helical edge magnon states: up and down magnons propagate along the edges of the sample in opposite directions. That is a bosonic analogue of the QSHE for electrons. Hence, an AF magnet in the presence of the Aharonov-Casher effect can be considered a magnonic topological insulator.

All these considerations were made assuming the system has a Néel ground state. In this work, we added an easy-axis anisotropy that ensures the magnetic Néel order is along the $\hat{\mathbf{z}}$ direction.

	Trivial transport (longitudinal)	Hall transport (transverse)
Magnetic field gradient	Spin current $\neq 0$ Heat current $= 0$	Spin current $= 0$ Heat current $\neq 0$
Thermal gradient	Spin current $= 0$ Heat current $\neq 0$	Spin current $\neq 0$ Heat current $= 0$

Table 1: Magnon transport induced by a magnetic field and thermal gradients in the topologically trivial and nontrivial bulk of the antiferromagnet described by Hamiltonian (8).

3 Transport

An electric field produces an electric current, and a magnetic field gradient gives rise to a spin current. Within the linear response theory, the Kubo formula for conductivity is given by [93, 96, 97]:

$$\sigma_{\alpha\beta}(\mathbf{q}, \omega) = -\frac{i}{V} \sum_{n,m} \sum_k \left(\frac{n_{n,k} - n_{m,k+q}}{E_{n,k} - E_{m,k+q}} \right) \frac{\langle \mathbf{k}, n | J_{\alpha,k} | \mathbf{k} + \mathbf{q}, m \rangle \langle \mathbf{k} + \mathbf{q}, m | J_{\beta,k+q} | \mathbf{k}, n \rangle}{\omega + i\eta + E_{n,k} - E_{m,k+q}} \quad (12)$$

where V is the volume; $J_{\alpha,k}$ is the current in the α direction at point \mathbf{k} of the Brillouin zone; $E_{n,k}$ is the energy of the n -th band and $n_{n,k}$ is the Fermi-Dirac distribution function for fermions or the Bose distribution function for bosons. The states $|\mathbf{k}, n\rangle$ in Eq. (12) are the exact eigenstates of the Hamiltonian and $E_{n,k}$ are the exact energy levels. However, in the spin wave approximation we use one-particle states of the noninteracting Hamiltonian.

The $\mathbf{q} = 0$ longitudinal magnon conductivity is given by:

$$\sigma_{xx}(\omega) = -\frac{i}{V} \sum_{n,m} \sum_k \left(\frac{n_{n,k} - n_{m,k}}{E_{n,k} - E_{m,k}} \right) \frac{\langle \mathbf{k}, n | J_{x,k} | \mathbf{k}, m \rangle \langle \mathbf{k}, m | J_{x,k} | \mathbf{k}, n \rangle}{\omega + i\eta + E_{n,k} - E_{m,k}} \quad (13)$$

The index n is identified with a band. We can perform the thermodynamic limit from discrete to continuous \mathbf{k} (where \mathbf{k} runs in each band). Besides the interband (regular) term, we have the additional intraband term (inside each band) where $m \rightarrow n$. Using

$$\frac{n_{n,k} - n_{m,k}}{E_{m,k} - E_{n,k}} = \frac{1}{\Delta} \left[n_{n,k} - \left(n_{n,k} + \frac{\partial n_{n,k}}{\partial E_{n,k}} \right) \Delta \right] = \frac{\partial n_{n,k}}{\partial E_{n,k}} \quad (14)$$

where $\Delta = E_m - E_n$, we get

$$\sigma_{xx}^{inband}(\omega) = \frac{1}{\omega + i\eta} \sum_k \frac{\partial n_{n,k}}{\partial E_{n,k}} \langle \mathbf{k}, n | J_{x,k} | \mathbf{k}, n \rangle \langle \mathbf{k}, n | J_{x,k} | \mathbf{k}, n \rangle \quad (15)$$

The real part of the dynamical spin conductivity $\sigma_{xx}(\omega)$ is written as

$$Re \sigma_{xx}(\omega) = D(T) \delta(\omega) + \sigma^{reg}(\omega) \quad (16)$$

Where the coefficient of the zero frequency δ function contribution is called the Drude weight, and it is given by

$$D(T) = \pi \sum_k \frac{\partial n_{n,k}}{\partial E_{n,k}} \langle \mathbf{k}, n | J_{x,k} | \mathbf{k}, n \rangle \langle \mathbf{k}, n | J_{x,k} | \mathbf{k}, n \rangle \quad (17)$$

This term is interpreted as the contribution of thermally excited particles propagating ballistically without interacting with other particles.

The regular part of the longitudinal conductivity σ_{xx}^{reg} is given by:

$$\sigma_{xx}^{reg}(\omega) = -\frac{1}{V} \sum_{n,m} \sum_k \left(\frac{n_{n,k} - n_{m,k}}{E_{n,k} - E_{m,k}} \right) \langle \mathbf{k}, n | J_{x,k} | \mathbf{k}, m \rangle \langle \mathbf{k}, m | J_{x,k} | \mathbf{k}, n \rangle \delta[\omega - (E_{n,k} - E_{m,k})] \quad (18)$$

The transverse static spin conductivity in a two-dimensional system, called the spin Hall conductivity, is

$$\sigma_{xy} = \sigma_{xy}(0,0) = \frac{i}{A} \sum_k \sum_{m \neq n} \frac{(n_{n,k} - n_{m,k}) \langle \mathbf{k}, n | J_{x,k} | \mathbf{k}, m \rangle \langle \mathbf{k}, m | J_{y,k} | \mathbf{k}, n \rangle}{[E_{n,k} - E_{m,k}] [E_{n,k} - E_{m,k} + i\eta]}, \quad (19)$$

where A is the area for a two-dimensional system. Using the formula for the spin current [22]:

$$J_\alpha = g\mu_B \frac{\partial H_k}{\partial k_\alpha}, \quad (20)$$

and defining

$$\Omega_{\alpha\beta}^n(\mathbf{k}) \equiv i \sum_{m \neq n} \frac{\langle \mathbf{k}, m | \partial H_k / \partial k_\alpha | \mathbf{k}, n \rangle \times \langle \mathbf{k}, n | \partial H_k / \partial k_\beta | \mathbf{k}, m \rangle}{(E_{m,k} - E_{n,k})^2} \quad (21)$$

the spin Hall conductivity σ_{xy} can be written as

$$\sigma_{xy} = (g\mu_B)^2 \sum_\lambda \int_{BZ} \frac{dk_x dk_y}{(2\pi)^2} n_k^\lambda \Omega_{xy}^\lambda(\mathbf{k}) \quad (22)$$

The term $\Omega_{xy}^\lambda(\mathbf{k})$ is the Berry curvature of the λ -th band (and from now on, the superscript indexes the bands). It is this term that gives rise to a transverse motion of magnons and leads to a Hall response. If H_k is real, there is always a choice to have real eigenvectors (unless there is a band degeneracy), which renders $\Omega_{xy}^\lambda(\mathbf{k}) = 0$. Therefore, the existence of an imaginary part of the Hamiltonian is a necessary condition to have a non-null Berry curvature. In the Union Jack lattice studied in Section 5, the imaginary part comes from the Dzyaloshinskii-Moriya term. In the brick-wall lattice studied in Section 8, it comes from a complex structure factor. Also, the gap should not vanish.

We can insert $\sum_{m'} |\mathbf{k}, m'\rangle \langle \mathbf{k}, m'| = I$ into Eq. (21) and obtain

$$\langle \mathbf{k}, n | \frac{\partial}{\partial k_\alpha} | \mathbf{k}, m' \rangle \langle \mathbf{k}, m' | H_k | \mathbf{k}, m \rangle \quad (23)$$

Renaming the eigenvectors as u_{nk} , it is easy to show that we can write

$$\Omega_{\alpha\beta}^n(\mathbf{k}) = i \left(\frac{\partial u_{nk}^\dagger}{\partial k_\alpha} \frac{\partial u_{nk}}{\partial k_\beta} - \frac{\partial u_{nk}^\dagger}{\partial k_\beta} \frac{\partial u_{nk}}{\partial k_\alpha} \right), \quad (\alpha, \beta = x, y) \quad (24)$$

or

$$\Omega_{xy}^n(\mathbf{k}) = i \sum_{\alpha\beta} \varepsilon_{\alpha\beta} \left(\frac{\partial u_{nk}^\dagger}{\partial k_\alpha} \frac{\partial u_{nk}}{\partial k_\beta} \right), \quad (\alpha, \beta = x, y) \quad (25)$$

where $n = 1, 2, \dots, N$ (N is the number of bands) and $\varepsilon_{\alpha\beta}$ is the antisymmetric tensor. The integral of the Berry curvature in the Brillouin zone, associated with band n , is the (first) Chern number $C^{(n)}$, which is an integer and temperature-independent so it cannot change its value continuously. Note that the Berry curvature measures the phase accumulated by the ground state eigenfunctions when evolving in the Brillouin zone. It is a local geometric object since it explicitly depends on \mathbf{k} . On the other hand, the Chern number is a global topological index. The sum of the Chern numbers over all bands is zero. The gap between neighboring bands has to be different from zero for systems with a non-null Chern number. However, a non-null gap does not imply a $C \neq 0$.

The Chern number is a topological invariant. That means that if we deform the energy bands (by varying the Hamiltonian parameters) without closing the gap, the Chern number will not change. Suppose that $C = 1$ in the bulk of a material. We have, naturally, $C = 0$ in the vacuum. In the very edge of the material, the Chern number has to change from $C = 1$ to $C = 0$, i.e., a topological phase transition. The localized states at the edge have to show gapless energy bands to allow that transition. Therefore, we have gapped bulk states and gapless edge states. We do not need to perform theoretical calculations in a finite sample to find out if we have gapless edge modes: the calculation of the Chern number in the bulk is sufficient.

In the case of fermions, if there exists an energy gap between the upper and lower bands, and the lower band is fully filled, that is $E_{-,k} < E_F < E_{+,k}$ (where E_F is the Fermi energy), then $f_{+,k} = 0$ and $f_{-,k} = 1$ at zero temperatures. Thus, the Hall conductivity of filled bands is given by

$$\sigma_{xy} = e^2 \sum_{n=filled} C^{(n)} \quad (26)$$

and is quantized. In the case of a magnon current, there are no filled bands, the Bose factor vanishes at zero temperature, and the current is not quantized. However, as mentioned above, a nonzero Chern number implies topologically protected edge states. The correspondence between the Chern number and the number of gapless edge states still holds for magnons.

4 Generalized Bogoliubov transformation

Here we present a formalism to diagonalize antiferromagnetic Hamiltonians. We start with a general quadratic bosonic Hamiltonian written in a matrix form as

$$H = \sum_k \psi_k^\dagger H_k \psi_k \quad (27)$$

where

$$\psi_k^\dagger = (b_{1k}^\dagger, \dots, b_{Nk}^\dagger, b_{1,-k}, \dots, b_{N,-k}) \quad (28)$$

We must diagonalize the matrix H_k to obtain the magnon spectrum. We need to find a transformation matrix T_k from a new basis φ_k to the old basis: $\psi_k = T_k \varphi_k$.

Let α_{mk} (α_{mk}^\dagger) be the eigenstates of H_k , and write

$$\varphi_k^\dagger = (\alpha_{1k}^\dagger, \dots, \alpha_{Nk}^\dagger, \alpha_{1,-k}, \dots, \alpha_{N,-k}) \quad (29)$$

After transformation, the components of φ_k must satisfy the same commutation relation as ψ_k , that is

$$[\varphi_{ik}, \varphi_{ik}^\dagger] = [\psi_{ik}, \psi_{ik}^\dagger] = \eta_{ij} \quad (30)$$

where

$$\eta = \begin{pmatrix} I_{N \times N} & 0 \\ 0 & -I_{N \times N} \end{pmatrix} \quad (31)$$

Here, $I_{N \times N}$ is a unit matrix. We must ensure that the commutation relations of the bosonic operators are conserved by the transformation T_k . The matrix T_k is chosen such that the Hamiltonian (27) can be written as

$$H = \sum_k \phi_k^\dagger T_k^\dagger H_k T_k \phi_k = \sum_k \phi_k^\dagger \tilde{H}_k \phi_k \quad (32)$$

where \tilde{H}_k is diagonal:

$$\tilde{H}_k = T_k^\dagger H_k T_k = \begin{pmatrix} \omega_{1k} & 0 & \dots & 0 \\ 0 & \omega_{2k} & \dots & 0 \\ \dots & \dots & \dots & \dots \\ 0 & 0 & \dots & \omega_{N,-k} \end{pmatrix} \quad (33)$$

In terms of the basis (29), Eq. (32) reads

$$H = \sum_k \sum_{n=1}^N \omega_{nk} \left(\alpha_{nk}^\dagger \alpha_{nk} + \frac{1}{2} \right) \quad (34)$$

To ensure that the new operators α_{nk} satisfy the bosonic algebra, the matrix T_k must fulfill the condition:

$$T_k \eta T_k^\dagger = \eta \quad (35)$$

A matrix T_k satisfying condition (35) is referred to as paraunitary.

The eigenvalues of H_k are obtained by the diagonalization of the matrix

$$K_k \equiv \eta H_k \quad (36)$$

The matrix K_k is non-Hermitian, but it can still be diagonalized by different left and right eigenstates with corresponding real eigenvalues. We should remember that a right eigenvector of a matrix A is a column matrix u that satisfies $Au = \lambda u$. A left eigenvector of A is a row matrix v that satisfies $vA = \lambda v$.

The matrix T_k consists of all the eigenvectors of K_k :

$$T = [V(\omega_1), \dots, V(\omega_N), V(-\omega_1), \dots, V(-\omega_N)] \quad (37)$$

with the eigenvectors V ordered as

$$V^\dagger(\omega_i) \eta V(\omega_i) = 1 \quad , \quad V^\dagger(-\omega_i) \eta V(-\omega_i) = -1 \quad (38)$$

for each set $(V(\omega_i), V(-\omega_i))$. The matrix T_k diagonalizes K_k and H_k simultaneously

$$T_k^{-1} K_k T_k \equiv \tilde{K}_k = \text{diag}[\omega_1, \dots, \omega_N, -\omega_1, \dots, -\omega_N] \quad (39)$$

$$T_k^\dagger H_k T_k \equiv \tilde{H}_k = \text{diag}[\omega_1, \dots, \omega_N, \omega_1, \dots, \omega_N] \quad (40)$$

From Eq. (38), we see there are two different normalizations for the eigenvectors of K_k . Also, all the eigenvalues are real and appear in pairs $\pm\omega_i$. It is usual to refer to the bands with indices $n = 1, \dots, N$ ($n = N+1, \dots, 2N$) as particle (hole) bands [25]. Particle states have normalization +1, while hole states have normalization -1. For more details, see Refs. [25, 98].

We also note that the Hamiltonian matrix H_k satisfies the particle-hole symmetry [23]:

$$H_k = \rho H_{-k}^T \rho; \quad \rho = \begin{pmatrix} 0 & I_{N \times N} \\ I_{N \times N} & 0 \end{pmatrix} \quad (41)$$

The procedure shown above establishes a specific order for the b_i^\dagger operators in ψ_k^\dagger (see Eq. (28)). But sometimes it is convenient to establish a different order. In general, we should write η as

$$\eta = \begin{pmatrix} \sigma_1 & 0 & 0 & 0 \\ 0 & \sigma_2 & 0 & 0 \\ 0 & 0 & \dots & 0 \\ 0 & 0 & 0 & \sigma_{2N} \end{pmatrix} \quad (42)$$

where $\sigma_i = +1$ (-1) if the correspondent operator in ψ_k^\dagger is b_k^\dagger (b_{-k}). That shuffles the particle/hole eigenvectors in T_k , but it can be useful if the corresponding matrix H_k is block-diagonal in this basis, which is the case of the Union Jack lattice.

In terms of the right and left eigenstates, we have:

$$\eta H_k |n, \mathbf{k}\rangle_R = (E_k)_{nn} |n, \mathbf{k}\rangle_R, \quad \langle n, \mathbf{k}|_L \eta H_k = (E_k)_{nn} \langle n, \mathbf{k}|_L \quad (43)$$

where

$$|n, \mathbf{k}\rangle_R = T_{n,k}, \quad \langle n, \mathbf{k}|_L = T_{n,k}^\dagger \quad (44)$$

We will use only the right eigenstate and write $|n, \mathbf{k}\rangle_R = |n, \mathbf{k}\rangle$. The normalization relation becomes

$$\langle n, \mathbf{k} | \eta | m, \mathbf{k} \rangle = \eta_{nm} \quad (45)$$

The Berry connection for a bosonic system is given by [28]

$$A_\alpha^n \equiv i \left[\eta T_k^\dagger \eta \frac{\partial T_k}{\partial k_\alpha} \right]_{nn} \quad (46)$$

Note that if the eigenstate of the n -th band is multiplied by a phase $e^{i\theta(\mathbf{k})}$ that is a smooth function of \mathbf{k} , then (46) transforms as $A_\alpha^n \rightarrow A_\alpha^n - \partial_{k_\alpha} \theta(\mathbf{k})$ under this phase change.

The Berry curvature is defined as

$$\Omega_{\alpha\beta}^n(\mathbf{k}) \equiv \frac{\partial A_{\beta}^n}{\partial k_{\alpha}} - \frac{\partial A_{\alpha}^n}{\partial k_{\beta}} \quad (47)$$

Using (46) we get [25]

$$\Omega_{xy}^n(\mathbf{k}) = i \sum_{\alpha\beta} \varepsilon_{\alpha\beta} \left[\eta \frac{\partial T_{\mathbf{k}}^{\dagger}}{\partial k_{\alpha}} \eta \frac{\partial T_{\mathbf{k}}}{\partial k_{\beta}} \right]_{nn}, \quad \alpha, \beta = x, y \quad (48)$$

The Berry curvature is gauge-invariant. Using Stoke's theorem, we see that the integral of the Berry curvature over the Brillouin zone is zero if $A_{\alpha}^n(\mathbf{k})$ is a smooth function across the zone. Only when it is impossible to parameterize the eigenstates over the entire Brillouin zone with a single gauge choice we get a nonzero Chern number. The sum of the Chern numbers over all particle and hole bands is individually zero [25].

In the Heisenberg picture, the operator $\psi_k(t)$ satisfies [27]

$$\frac{d\psi_k}{dt} = \frac{i}{\hbar} [\psi_k^{\dagger} H_k \psi_k, \psi_k] = \frac{i}{\hbar} [\psi_k^{\dagger}, \psi_k] H_k \psi_k = -\frac{i}{\hbar} \eta H_k \psi_k \quad (49)$$

That is, $\psi_k(t)$ is the solution of a non-Hermitian Schrödinger-like equation

$$i\hbar \frac{d\psi_k}{dt} = \eta H_k \psi_k \quad (50)$$

The non-Hermiticity modifies the inner product for the boson wave functions as $\langle \phi_a | \phi_b \rangle = \phi_a^{\dagger} \eta \phi_b$.

5 The Union Jack Lattice

Thermal Hall conductivity in antiferromagnets is studied mainly in the kagome [71, 72, 75] and honeycomb [49, 68, 69] geometry, but it has already been investigated in the square [25, 29], checkerboard [87, 88] and variations of the Lieb lattices [89–91]. Using the Schwinger boson mean-field theory, Samajdar et al. [25] extended the calculations to spin-liquids. With the intent to find novel antiferromagnetic systems where Hall-like transport is present, here we study a two-dimensional AF Union Jack lattice with the Hamiltonian given by:

$$\begin{aligned} H = & J_1 \sum_{\langle i,j \rangle} \mathbf{S}_i \cdot \mathbf{S}_j + \sum_{\langle\langle i,i' \rangle\rangle} J_{2,ii'} (\mathbf{S}_i \cdot \mathbf{S}_{i'} + (\lambda - 1) S_i^z S_{i'}^z) + \\ & + D \sum_{\langle i,j \rangle} \nu_{ij} \hat{\mathbf{z}} \cdot \mathbf{S}_i \times \mathbf{S}_j - A \sum_i (S_i^z)^2 \end{aligned} \quad (51)$$

We obtain the Union Jack lattice by adding alternate diagonals to the square lattice (Figure 1). The lattice is divided into A and B sublattices, denoted by indices i and j , respectively. Here $\langle i, j \rangle$ means the near-neighbor (NN) spins with exchange interaction between sites A and B, and $\langle\langle i, i' \rangle\rangle$ means next-near-neighbor (NNN) interactions between sites AA. The NNN exchange interaction carries two kinds of anisotropy: an off-plane $\lambda > 1$ anisotropy which favors the alignment of the spins in the $\hat{\mathbf{z}}$ direction; and an in-plane anisotropy in the form of different exchange constants $J_{2,ii'}$ for different in-plane directions ($J_{2,x} = J_2$ and $J_{2,y} = \alpha J_2$).

The third term of the Hamiltonian is the spin-orbit-induced Dzyaloshinskii-Moriya interaction (DMI) between sites A and B. It has become well established that DMI is the primary source of topological magnon effects in quantum magnets. The term has the general form $\mathbf{D}_{ij} \cdot \mathbf{S}_i \times \mathbf{S}_j$ with $\mathbf{D}_{ij} = -\mathbf{D}_{ji}$. We take the interaction along the $\hat{\mathbf{z}}$ direction so that $\mathbf{D}_{ij} = D\nu_{ij}\hat{\mathbf{z}}$ with $\nu_{ij} = \pm 1$ for different bond orientations (see Figure 1). For sufficiently large D (comparable to J_1) the ground state is no longer a collinear antiferromagnet but a spin spiral. The magnetic sublattices tilt away from their antiparallel alignment, forming a net magnetic moment known as weak ferromagnetic moment. Therefore, we will consider only small D values compared to J_1 , which would preserve the Néel ground state.

The occurrence of DMI requires that the spatial inversion symmetry of the crystal field surrounding the magnetic ions be broken. Hence, the conventional DM term is absent if the crystal lattice is centrosymmetric. However, this term can be induced by an external electric field, which has the advantage that the strength of the field can be tuned [99].

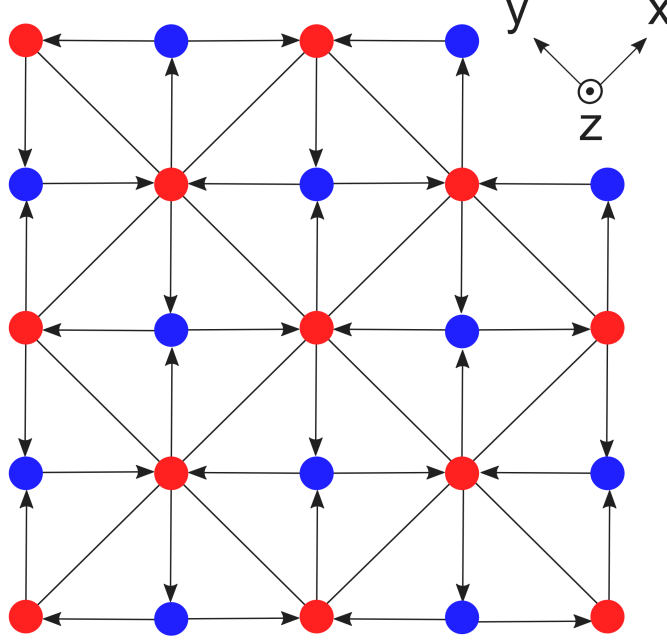


Figure 1: The Union Jack lattice. Red (blue) circles represent the A (B) sublattice. The sign of the DM interaction is $\nu_{ij} = +1(-1)$ if i, j is following (against) the arrows.

When the DM term is imaginary in the reciprocal space Hamiltonian, we have an analogue of the Aharonov-Casher effect mentioned in Section 2, with $\mathbf{D}_{ij} \propto \mathbf{E} \times \hat{\mathbf{e}}_{ij}$ (where $\hat{\mathbf{e}}_{ij}$ is the unit vector connecting the two sites i and j). In this case, the DMI contributes to the Berry curvature and is responsible for the Lorentz force acting on the propagating magnons (the DM vector acts as the vector potential or a gauge field to the spin current). That is what happens in the Union Jack lattice. On the other hand, if the DM term is real, it does not contribute to the Berry curvature. As we need an imaginary term in the Hamiltonian for a non-null Berry curvature, it has to come from another term, such as the structure factor of the exchange interaction. This is the case of the honeycomb and brick-wall lattices (see Section 8), where we have a non-null Berry curvature even without DM interaction.

The last term in Hamiltonian (51) is a single ion easy-axis anisotropy (SIA) which favors spin alignment along the $\hat{\mathbf{z}}$ direction. Magnetic anisotropy is crucial to overcome thermal fluctuations and stabilize the magnetic order. Since the Hamiltonian is invariant under global spin rotation about the z-axis, the $\hat{\mathbf{z}}$ component of the total spin is conserved.

We set the spacing of each sublattice equal to 1, and take the $\hat{\mathbf{x}}$ and $\hat{\mathbf{y}}$ directions along the diagonal axes of the two sublattices since the lattice is translationally invariant along the diagonals. The Hamiltonian (51) with $A = D = 0$ and $\lambda = \alpha = 1$ was studied by Collins et al. [100] at zero temperature. For these values of parameters, our calculations agree with the ones performed by them. The lattice is frustrated, and in particular, there is a phase transition from an ordered Néel phase to a canted ferrimagnetic phase at $\eta_c = J_2/J_1 \approx 0.65$ for spin 1/2 [101, 102] and $\eta_c \approx 0.58$ for $S = 1$ [103]. Hence, we restrict the values of the parameters to the regime where the Néel order is preserved. The term $A > 0$ favors easy-axis alignment along the z-axis and leads to an ordered phase below the transition temperature T_N .

As usual, we take the Néel order perpendicular to the lattice plane, i. e., spins on the A and B sublattices satisfy $\mathbf{S}_A = -\mathbf{S}_B = S\hat{\mathbf{z}}$ in the ground state. We use the linearized Holstein-Primakoff representation for antiferromagnets

$$\begin{aligned}
S_i^+ &= \sqrt{2S}a_i, \quad S_i^- = \sqrt{2S}a_i^\dagger, \quad S_i^z = S - a_i^\dagger a_i & i \in A \\
S_j^+ &= \sqrt{2S}b_j^\dagger, \quad S_j^- = \sqrt{2S}b_j, \quad S_j^z = -S + b_j^\dagger b_j & j \in B
\end{aligned} \tag{52}$$

The magnetic excitations can be described as chargeless bosonic quasiparticles (magnons) carrying a dipole momentum $\sigma g \mu_B \hat{\mathbf{e}}_{\mathbf{z}}$ with $\sigma = \pm 1$. Since we are considering only single-magnon excitations, the average magnon number on each spin is much smaller than $2S$. The approximation is valid when the spin magnitude S is large and/or the temperature is low enough, such that the population of thermally activated magnons at each site becomes small. However, the theory was used to fit experimental data in an $S = 1/2$ compound and remarkably gave better results than the Schwinger boson representation, even above the transition temperature [60].

We perform a Bogoliubov transformation from bosons (a_i, b_i) to (α_i, β_i) (see Section 4). Using Eqs. (52) and (A.26) we can show that

$$S^z = \sum_{i \in A} \sum_{j \in B} (S_i^z + S_j^z) = \sum_k \left(-\alpha_k^\dagger \alpha_k + \beta_k^\dagger \beta_k \right) \tag{53}$$

Hence $\langle 0 | \alpha_k S^z \alpha_k^\dagger | 0 \rangle = -1$ and $\langle 0 | \beta_k S^z \beta_k^\dagger | 0 \rangle = +1$ (where $|0\rangle$ is the magnon vacuum), showing that α magnons carry -1 spin angular momentum and β magnons carry $+1$ spin angular momentum along the $\hat{\mathbf{z}}$ direction [68]. Momentum and spin conservations are fulfilled by a combination of α and β magnons, which carry opposite spins and momenta (\mathbf{k} and $-\mathbf{k}$). Note that the magnon operators α and β are a mixture of a and b operators (which are not magnon operators), and therefore are not associated to sublattices A and B.

Taking Eq. (52) into the Hamiltonian (51) and Fourier transforming, we obtain (after discarding the zero-point energy and higher order terms) the following quadratic Hamiltonian:

$$H = H_1 + H_2 + H_{DM} + H_{SIA} \tag{54}$$

where

$$H_1 = 2J_1 S \sum_k \left[a_k^\dagger a_k + a_k a_k^\dagger + b_k^\dagger b_k + b_k b_k^\dagger + \gamma_k \left(a_k b_{-k} + b_{-k} a_k + a_k^\dagger b_{-k}^\dagger + b_{-k}^\dagger a_k^\dagger \right) \right] \tag{55}$$

$$H_2 = S J_2 \sum_k \left[(2\eta_k - \lambda(\alpha + 1)) \left(a_k^\dagger a_k + a_k a_k^\dagger \right) \right] \tag{56}$$

$$H_{DM} = 2iSD \sum_k m_k \left[(a_k b_{-k} + b_{-k} a_k) - \left(a_k^\dagger b_{-k}^\dagger + b_{-k}^\dagger a_k^\dagger \right) \right] \tag{57}$$

$$H_{SIA} = \frac{1}{2} A (2S - 1) \sum_k \left(a_k^\dagger a_k + a_k a_k^\dagger + b_k^\dagger b_k + b_k b_k^\dagger \right) \tag{58}$$

with the structure factors defined as

$$\gamma_k = \cos \frac{k_x}{2} \cos \frac{k_y}{2}, \quad \eta_k = \frac{1}{2} (\cos k_x + \alpha \cos k_y), \quad m_k = -\sin \frac{k_x}{2} \sin \frac{k_y}{2} \tag{59}$$

For the appearance of the term $(2S - 1)$ in Eq. (58) see Eq. (A.7). We see that for $S = 1/2$, we have $H_{SIA} = 0$ and the single-ion anisotropy is not effective.

We show the calculation explicitly for m_k considering the factor ν_{ij} as $+1$ in the up/down direction and -1 in the left/right direction, departing from an A site (see Figure (1)):

$$m_k = \frac{1}{4} \left(e^{i(k_x + k_y)/2} - e^{i(-k_x + k_y)/2} - e^{i(k_x - k_y)/2} + e^{-i(k_x + k_y)/2} \right) = -\sin \frac{k_x}{2} \sin \frac{k_y}{2} \tag{60}$$

As mentioned above, the spin wave formalism, although widely used in the literature, is justified only for large spin values and low temperatures. Note, however, that our calculations are valid for any spin value.

To present a general discussion of an antiferromagnet, we write the Hamiltonian (51) as

$$H = \sum_k \left(M_{11} a_k^\dagger a_k + M_{12} a_{-k}^\dagger b_k^\dagger + M_{21} b_{-k} a_k + M_{22} b_k b_k^\dagger + M_{33} a_k a_k^\dagger + \right. \\ \left. + M_{34} a_{-k} b_k + M_{43} b_{-k}^\dagger a_k^\dagger + M_{44} b_k^\dagger b_k \right) \quad (61)$$

This can be written as

$$H = \sum_k \psi_k^\dagger H_k \psi_k \quad (62)$$

Here, for convenience, we use a different convention than that used in Eq. (28), and write $\psi_k^\dagger = \begin{pmatrix} a_k^\dagger & b_{-k} & a_{-k} & b_k^\dagger \end{pmatrix}$. This k-space basis is similar to the one used in Ref. [69]. As a result, the matrix H_k splits in two blocks:

$$H_k = \begin{pmatrix} M_k & 0 \\ 0 & M_{-k}^* \end{pmatrix}, \quad \text{where } M_k = \begin{pmatrix} r_{1k} & f_k^* \\ f_k & r_{2k} \end{pmatrix} \quad (63)$$

We can notice that the \mathbf{k} dependence comes only from the structure factors γ_k , η_k and m_k . For the Union Jack lattice as studied here, these factors are even functions of \mathbf{k} . Hence, $M_k = M_{-k}$ and we can ignore the sign of \mathbf{k} in the Hamiltonian parameters. We identify

$$M_{11} = r_{1k}, \quad M_{22} = r_{2k}, \quad M_{21} = f_k = h_{xk} + i h_{yk}, \quad M_{12} = f_k^* = h_{xk} - i h_{yk} \quad (64)$$

Specifically for the Union Jack lattice, we have:

$$r_{1k} = S [2J_1 + J_2 (2\eta_k - \lambda(\alpha + 1))] + \frac{1}{2} A (2S - 1) \\ r_{2k} = 2S J_1 + \frac{1}{2} A (2S - 1) \\ h_{xk} = 2S J_1 \gamma_k \\ h_{yk} = 2SD m_k \quad (65)$$

A Hamiltonian with particle-hole symmetry is known as the Bogoliubov-de Gennes (BdG) Hamiltonian and is written as

$$H_{BdG} = \begin{pmatrix} \Xi_k & \Lambda_k \\ \Lambda_{-k}^* & \Xi_{-k}^* \end{pmatrix} \quad (66)$$

where Ξ_k and Λ_k are 2×2 matrices. The Hamiltonian for the AF honeycomb [49, 68–70] and square [31] lattices can be written this way. For the Union Jack lattice, we see that $\Xi_k = M_k$ and $\Lambda_k = 0$.

From Eq. (63), and noting the specific order of the operators in ψ_k^\dagger , we have

$$\eta = \text{diag}(1, -1, -1, 1) = \begin{pmatrix} \sigma_z & 0 \\ 0 & -\sigma_z \end{pmatrix} \quad (67)$$

The advantage of working with a block-diagonal Hamiltonian is evident when we write K_k as

$$K_k = \eta H_k = \begin{pmatrix} \sigma_z M_k & 0 \\ 0 & -\sigma_z M_{-k}^* \end{pmatrix} \quad (68)$$

We can, then, diagonalize the sectors of K_k separately. The first sector, which we call α -sector, has eigenvectors

$$\varphi_\alpha^{(+)} = \begin{pmatrix} u_k^* \\ -v_k^* \end{pmatrix}, \quad \varphi_\alpha^{(-)} = \begin{pmatrix} -v_k \\ u_k \end{pmatrix} \quad (69)$$

with corresponding eigenvalues

$$\omega_\alpha^{(+)}(\mathbf{k}) = w(\mathbf{k}) + \Delta(\mathbf{k}), \quad \omega_\alpha^{(-)}(\mathbf{k}) = -w(\mathbf{k}) + \Delta(\mathbf{k})$$

The parameters u and v are defined as

$$u = \frac{f}{|f|} \left(\frac{r+w}{2w} \right)^{1/2}, \quad v = v^* = \left(\frac{r-w}{2w} \right)^{1/2} \quad (70)$$

with

$$r = \frac{r_1 + r_2}{2}, \quad \Delta = \frac{r_1 - r_2}{2}, \quad w = \sqrt{r^2 - |f|^2} \quad (71)$$

The eigenvectors of the α -sector can also be written as [49]

$$\varphi_\alpha^{(+)} = \begin{pmatrix} e^{-i\phi} \cosh \frac{\theta}{2} \\ -\sinh \frac{\theta}{2} \end{pmatrix}, \quad \varphi_\alpha^{(-)} = \begin{pmatrix} -\sinh \frac{\theta}{2} \\ e^{i\phi} \cosh \frac{\theta}{2} \end{pmatrix} \quad (72)$$

where the new parameters ϕ and θ are defined as

$$\tan \phi = \frac{h_y}{h_x}, \quad \cosh \theta = \frac{r}{w} \quad (73)$$

This form is particularly useful to obtain an expression for the Berry curvature, as it will be shown later. We note that

$$e^{i\phi} = \frac{f}{|f|}, \quad \cosh \frac{\theta}{2} = \left(\frac{r+w}{2w} \right)^{1/2}, \quad \sinh \frac{\theta}{2} = \left(\frac{r-w}{2w} \right)^{1/2} \quad (74)$$

There is a degree of freedom in choosing the eigenvectors, which are related by $U(1)$ gauge transformations. That is, the eigenstates can be written in two ways related by a phase $e^{i\phi}$. However, the gauge does not affect the Berry curvature.

The eigenvectors of the β -sector (second block of H_k) are the complex conjugate of the α -sector with a substitution $\mathbf{k} \rightarrow -\mathbf{k}$. The eigenvalues are:

$$\omega_\beta^{(+)}(\mathbf{k}) = w(-\mathbf{k}) - \Delta(-\mathbf{k}), \quad \omega_\beta^{(-)}(\mathbf{k}) = -w(-\mathbf{k}) - \Delta(-\mathbf{k})$$

As we saw before, a quantum of α -magnon carries spin -1 and a quantum of β -magnon a spin $+1$. The transformation doubles the Hilbert space, so the eigenvalues of K_k show up in pairs $\pm\omega(\pm\mathbf{k})$. For bosons, only positive energy states are physical, and we keep only the positive branches $\varphi_\alpha^{(+)}$ and $\varphi_\beta^{(+)}$ [25]. Nevertheless, when using the Kubo formula we must perform the calculations in the full particle-hole space. Then, using the particle-hole symmetry we can express our result only in terms of the positive energy states [12]. The matrix T_k , which diagonalizes K_k and carries all four eigenvectors is:

$$\begin{aligned} T_k &= \begin{pmatrix} u_k^* & -v_k & 0 & 0 \\ -v_k^* & u_k & 0 & 0 \\ 0 & 0 & u_{-k} & -v_{-k}^* \\ 0 & 0 & -v_{-k} & u_{-k}^* \end{pmatrix} \\ &= \begin{pmatrix} e^{-i\phi_k} \cosh \frac{\theta_k}{2} & -\sinh \frac{\theta_k}{2} & 0 & 0 \\ -\sinh \frac{\theta_k}{2} & e^{i\phi_k} \cosh \frac{\theta_k}{2} & 0 & 0 \\ 0 & 0 & e^{i\phi_{-k}} \cosh \frac{\theta_{-k}}{2} & -\sinh \frac{\theta_{-k}}{2} \\ 0 & 0 & -\sinh \frac{\theta_{-k}}{2} & e^{-i\phi_{-k}} \cosh \frac{\theta_{-k}}{2} \end{pmatrix} \\ &= \left(\varphi_\alpha^{(+)}, \varphi_\alpha^{(-)}, \varphi_\beta^{(-)}, \varphi_\beta^{(+)} \right) \end{aligned} \quad (75)$$

and the diagonalized K_k , which carries the eigenvalues, is:

$$E_k \equiv T_k^{-1} K_k T_k = \begin{pmatrix} \omega_\alpha^{(+)}(\mathbf{k}) & 0 & 0 & 0 \\ 0 & \omega_\alpha^{(-)}(\mathbf{k}) & 0 & 0 \\ 0 & 0 & \omega_\beta^{(-)}(\mathbf{k}) & 0 \\ 0 & 0 & 0 & \omega_\beta^{(+)}(\mathbf{k}) \end{pmatrix}$$

The positive energy spectrum is given by:

$$\begin{aligned} E_{\alpha}^{(+)} / \hbar &= \omega_{\alpha}^{(+)}(\mathbf{k}) = w(\mathbf{k}) + \Delta(\mathbf{k}) \\ E_{\beta}^{(+)} / \hbar &= \omega_{\beta}^{(+)}(\mathbf{k}) = w(-\mathbf{k}) - \Delta(-\mathbf{k}) \end{aligned} \quad (76)$$

Here, the particle states correspond to T_k 's first and fourth columns. That comes from the specific order of the operators chosen in the vector $\psi_k^{\dagger} = (a_k^{\dagger} \ b_{-k} \ a_{-k} \ b_k^{\dagger})$. The second and third columns represent the hole states with a negative energy spectrum (non-physical). We analyze the band structure in the following.

For the Union Jack lattice we can ignore the minus sign in the argument of the functions in the β -sector, as all the structure factors are even in \mathbf{k} (See Eq. (59)). With definitions (65) and (71), we see that

$$\Delta(\mathbf{k}) = \frac{r_1 - r_2}{2} = \frac{1}{2} S J_2 [2\eta_k - \lambda(\alpha + 1)] \quad (77)$$

If $J_2 = 0$ the term Δ vanishes, and the magnon bands are degenerate. The system is reduced to the AF square lattice [7]. Higher values of J_2 lower the band of the α -mode, while the β -mode band remains almost unchanged (Figure 2).

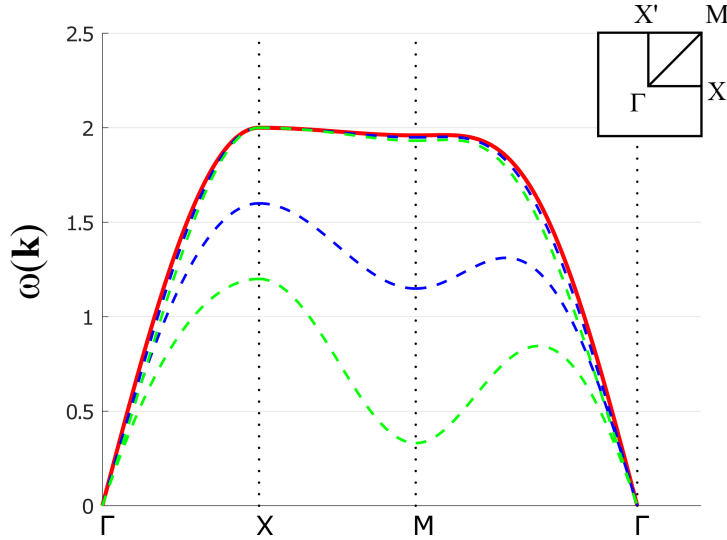


Figure 2: Energy bands of the AF Union Jack lattice for three values of J_2/J_1 : 0 (square lattice, solid red, both bands are totally degenerate), 0.2 (dashed blue) and 0.4 (dashed green). Other parameters are $S = J_1 = \lambda = \alpha = 1$, $A = 0$, $D = 0.2$. Both bands have a null gap.

For small enough values of A/J_1 , J_2/J_1 and D/J_1 both bands have a minimum at $k_x = k_y = 0$ (Γ point). This minimum defines the bands' gaps:

$$\omega_{gap}^{\alpha,\beta} = w_0 \pm \Delta_0 \quad (78)$$

with

$$\Delta_0 = \frac{1}{2} S J_2 (\alpha + 1) (1 - \lambda) \quad (79)$$

We see that for $\lambda = 1$ we have $\Delta_0 = 0$, and the gap has the same value w_0 for both bands, meaning there is a degeneracy at point Γ . In this picture, we have:

$$\omega_{gap}|_{\lambda=1} = \frac{1}{2} \sqrt{A(2S-1)} \sqrt{8SJ_1 + A(2S-1)} \quad (80)$$

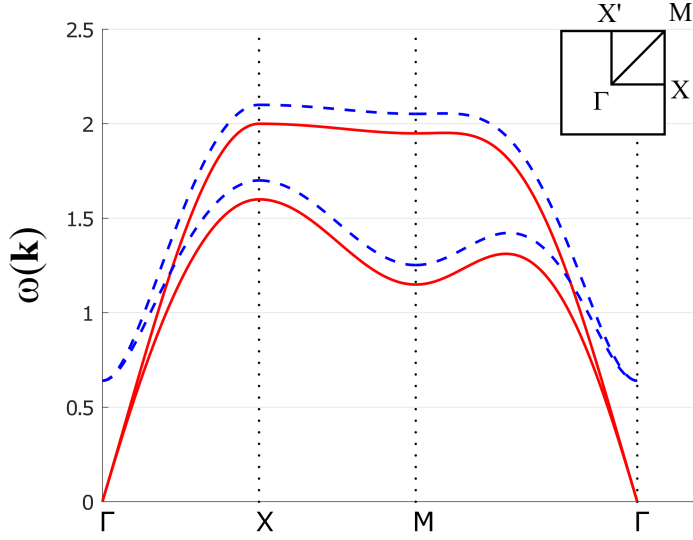


Figure 3: Energy bands of the AF Union Jack lattice with $A = 0$ (solid red) and $A = 0.2$ (dashed blue). Other parameters are $S = J_1 = \lambda = \alpha = 1$, $J_2 = D = 0.2$. The SIA opens the gap, but bands are still degenerate at point Γ .

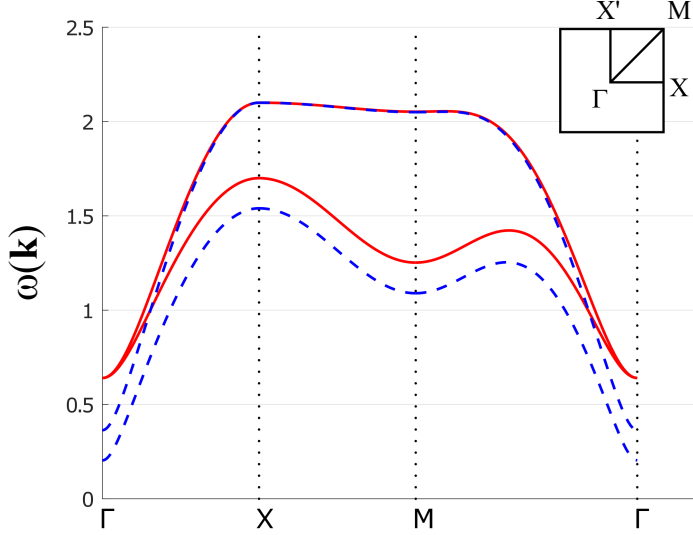


Figure 4: Dispersion curves of the AF Union Jack lattice for $\lambda = 1$ (solid red) and $\lambda = 1.4$ (dashed blue). Other parameters are $S = J_1 = \alpha = 1$, $J_2 = A = D = 0.2$. The off-plane exchange anisotropy λ splits and lowers the bands at point Γ .

The gap vanishes only for $A = 0$ or $S = 1/2$. In other words, the *SIA* term opens the gap at the Γ point (Figure 3), while the off-plane exchange anisotropy λ makes the gap different for each magnon, splitting the bands at this point (Figure 4). For any $T > 0$, a null gap $\omega(\mathbf{k}_0) = 0$ makes the magnon population explode at point \mathbf{k}_0 , resulting in divergent Berry curvature. Hence, we need $A \neq 0$ and $S \neq 1/2$ for well-behaved Berry curvature and transverse transport coefficients,. The non-null gap stabilizes the ground state as it becomes energetically isolated from the rest of the spectrum.

The effect of the in-plane α anisotropy is to create an energetic inequivalence between points X and X' of the Brillouin zone (Figure 5). This energetic imbalance enables non-null transverse transport. We also note

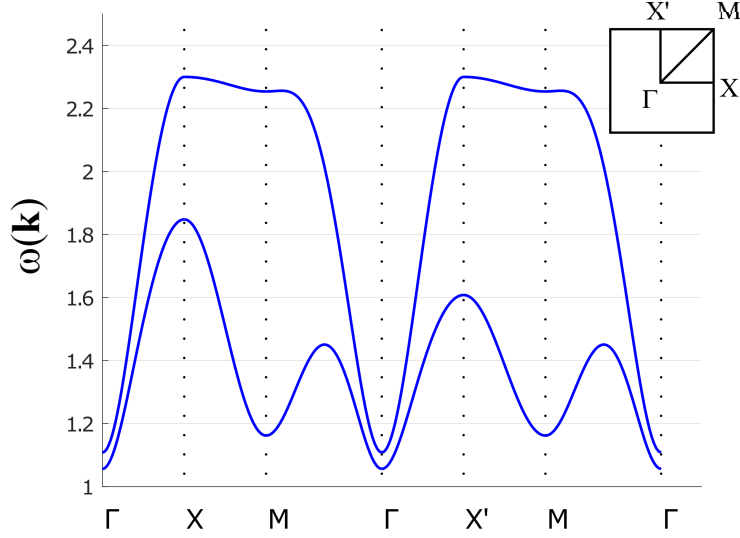


Figure 5: The effect of the in-plane exchange anisotropy α on the AF Union Jack lattice is to create an energetic inequivalence between points axes k_x and k_y . The parameters are $S = J_1 = 1$, $J_2 = D = 0.2$, $A = 0.6$, $\lambda = 1.1$, $\alpha = 1.6$.

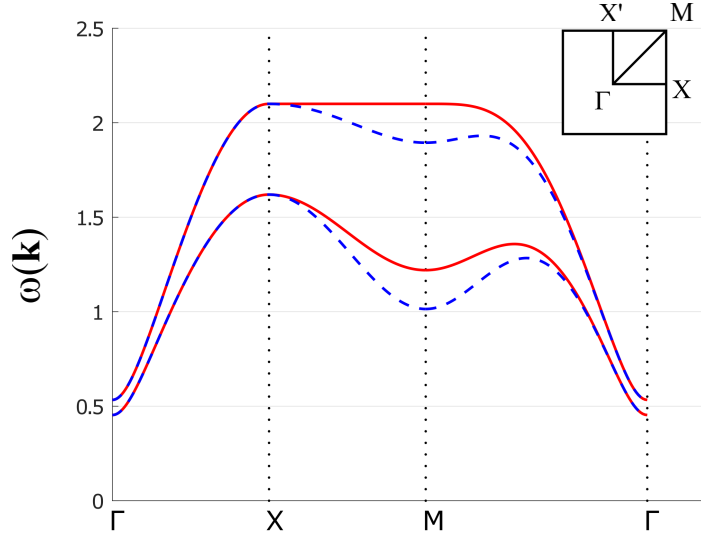


Figure 6: Effect of the DM interaction on the dispersion curves of the AF Union Jack lattice. The solid red line is the $D = 0$ case, while the blue dashed line is the $D = 0.4$ case. Other parameters are $S = J_1 = \alpha = 1$, $J_2 = A = 0.2$, $\lambda = 1.2$.

that the DMI itself doesn't open a gap, but changes the character of the dispersion by lowering the energy at the point M (Figure 6).

We also studied the effect of the anharmonic contributions (magnon-magnon interactions) in a mean-field picture, where the Hamiltonian is renormalized by temperature-dependent parameters. In this modified spin wave (MSW) approach, even at zero temperature, the anharmonic contributions affect the energy bands, lowering the bands' gap (Figure 7). As the temperature rises, the bands remain virtually unchanged until we get closer to the Néel temperature T_N , when the energy drops abruptly (Figure 8). At T_N the Néel order is unstable, and the staggered magnetization vanishes, signaling a phase transition (Figure 9). The transition temperature T_N tends to be higher for high values of A or S . A complete description and the analytical results of the MSW

approach can be found in Appendix A.

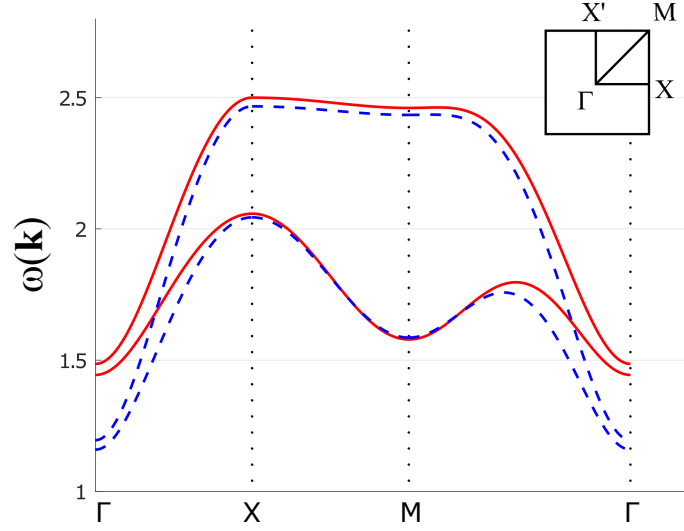


Figure 7: Linear spin wave dispersion relation (LSW, solid red line) compared to the modified spin wave case (MSW, dashed blue line) in the Union Jack lattice. The temperature is zero, parameters are $S = J_1 = A = 1$, $J_2 = D = 0.2$, $\lambda = \alpha = 1.1$. The MSW lowers the gap even at zero temperature.

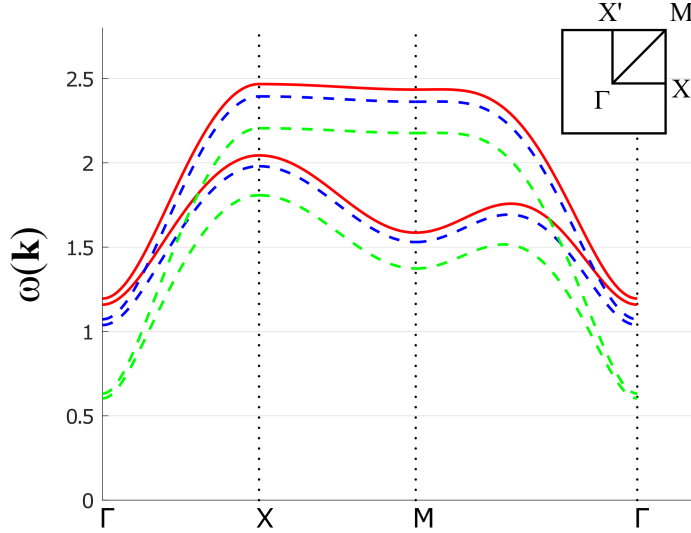


Figure 8: MSW dispersion for $T = 0$ (solid red), $T = 0.4$ (dashed blue) and $T = 0.455$ (dashed green) in the Union Jack lattice. The gap shrinks abruptly as we approach the transition temperature $T_N \approx 0.456$. The parameters are $S = J_1 = A = 1$, $J_2 = D = 0.2$, $\lambda = \alpha = 1.1$.

6 Symmetries

Crystal structures can be classified by the symmetries they present. An ideal crystal is a periodically repeating pattern. Since all lattice points of a periodic lattice are equivalent, every point has the same neighborhood as other points. So the lattice itself can be characterized by listing the symmetry operations that keep each of

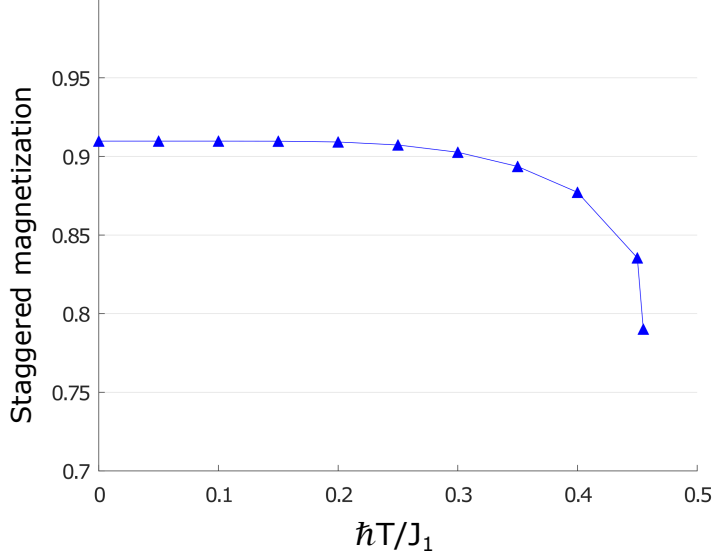


Figure 9: Staggered magnetization for MSW on the Union Jack lattice. The parameters are $S = J_1 = A = 1, J_2 = D = 0.2, \lambda = \alpha = 1.1$. The Néel temperature was estimated in $T_N \approx 0.456$.

them fixed [10]. The point symmetries are rotations c_n (due to periodicity, rotations are restricted to be $360^\circ/n$, where $n = 1, 2, 3, 4, 6$), reflections, space inversions, and combinations of them. Space inversion maps $\mathbf{r} \rightarrow -\mathbf{r}$ and $\mathbf{k} \rightarrow -\mathbf{k}$. When we have magnetic ordering, the crystallographic symmetries can be extended to describe magnetic crystals. Spatial inversion symmetry implies $\omega(\mathbf{k}) = \omega(-\mathbf{k})$.

The time-reversal operation \mathcal{T} inverts all spins, changes \mathbf{k} into $-\mathbf{k}$ and takes the complex conjugate. Note that a Hamiltonian can be invariant under TRS, but the symmetry can be spontaneously broken in the ground state. In an antiferromagnet with Néel order TRS is broken, since flipping all the spins would swap the A and B sublattices, changing the sign of the staggered magnetization. Another symmetry is broken, namely, the symmetry under lattice translation $T_{\mathbf{a}}$, where \mathbf{a} is a vector connecting two sublattices in the case of a bipartite antiferromagnet. In general, time-reversal symmetry can be effectively restored if another symmetry \mathcal{S} of the Hamiltonian, combined with the TRS, is a good symmetry of the system. For instance, besides translation, the Hamiltonian can also remain invariant under the combined time-reversal and spin rotation ($\mathcal{S} = c_x$) by 180° around the x-axis (or any other in-plane axis). These combined symmetries operations \mathcal{TS} are sometimes called effective time-reversal symmetry (ETRS).

To understand the symmetry properties of the ground state of the Heisenberg antiferromagnet, we follow Cheng et al. [68] and start with the Néel ground state. We write

$$\begin{aligned}
H &= J_1 \sum_{\langle A, B \rangle} \mathbf{S}_A \cdot \mathbf{S}_B + J_2 \sum_{\langle\langle A, A' \rangle\rangle} \mathbf{S}_A \cdot \mathbf{S}_{A'} + \mathcal{K} \sum_{A, B} \left[(S_A^z)^2 + (S_B^z)^2 \right] \\
&= H_1 + H_2 + H_{SIA}
\end{aligned} \tag{81}$$

where J_1 is an exchange interaction between NN sites of different sublattices, and J_2 is between NNN of the same sublattice A (it could as well be sublattice B). Writing $\mathbf{S}_A = \delta \mathbf{S}_A + \hat{\mathbf{z}}$ and $\mathbf{S}_B = \delta \mathbf{S}_B - \hat{\mathbf{z}}$, we have

$$\begin{aligned}
\mathbf{S}_A \cdot \mathbf{S}_B &= (\delta \mathbf{S}_A + \hat{\mathbf{z}}) \cdot (\delta \mathbf{S}_B - \hat{\mathbf{z}}) = \delta \mathbf{S}_A \cdot \delta \mathbf{S}_B - \delta S_A^z + \delta S_B^z - 1 \\
\mathbf{S}_A \cdot \mathbf{S}_{A'} &= (\delta \mathbf{S}_A + \hat{\mathbf{z}}) \cdot (\delta \mathbf{S}_{A'} + \hat{\mathbf{z}}) = \delta \mathbf{S}_A \cdot \delta \mathbf{S}_{A'} + \delta S_A^z + \delta S_{A'}^z + 1 \\
(S_A^z)^2 + (S_B^z)^2 &= (\delta S_A^z)^2 + (\delta S_B^z)^2 + 2(1 + \delta S_A^z - \delta S_B^z)
\end{aligned} \tag{82}$$

As we are interested in the symmetry properties of magnons, all symmetry operations act only on the perturbations $\delta \mathbf{S}_{A, B}$, leaving the Néel ground state unchanged [68]. The time-reversal operation \mathcal{T} changes the sign of all components of $\delta \mathbf{S}$. The spin rotation c_x (by 180°) only changes the sign of δS^y and δS^z , leaving δS^x

unchanged. Hence, the combined symmetry $\mathcal{T}c_x$ have the effect of changing the sign of δS^x . From Eq. (82), we can see that $H_1 + H_2 + H_{SIA}$ is invariant under the $\mathcal{T}c_x$. This is the ETRS of the system.

Let us now consider the DM term

$$H_{DM} = D \sum_{i,j} \nu_{ij} (S_i^x S_j^y - S_i^y S_j^x) \quad (83)$$

Making the same substitution as before, we obtain

$$H_{DM} = D \sum_{i,j} \nu_{ij} (\delta S_i^x \delta S_j^y - \delta S_i^y \delta S_j^x) \quad (84)$$

As $\mathcal{T}c_x$ changes the sign of δS^x , the DMI breaks the ETRS of the Hamiltonian. It is indifferent if the interaction is between sites of the same or different sublattices because the operation acts similarly in both $\delta \mathbf{S}_A$ and $\delta \mathbf{S}_B$.

The developments above are made under the assumption of a Néel ground state, but it is known that the DMI can bend the spins, generating a canted ground state. Even in a canted collinear antiferromagnet, the canting explicitly breaks time-reversal symmetry, whereas the Dzyaloshinskii-Moriya interaction provides the necessary Lorentz force on the magnons.

7 Berry curvature and transverse transport

The Berry curvature of a system described by a Hamiltonian like Eq. (63) can be found analytically from the Hamiltonian parameters. From Eqs. (48) and (75), we can show that (see Appendix B):

$$\begin{aligned} \Omega^\alpha(\mathbf{k}) &= -\frac{1}{2} \sinh \theta_k \left(\frac{\partial \phi_k}{\partial k_x} \frac{\partial \theta_k}{\partial k_y} - \frac{\partial \phi_k}{\partial k_y} \frac{\partial \theta_k}{\partial k_x} \right) \\ \Omega^\beta(\mathbf{k}) &= -\frac{1}{2} \sinh \theta_{-k} \left(\frac{\partial \phi_{-k}}{\partial k_x} \frac{\partial \theta_{-k}}{\partial k_y} - \frac{\partial \phi_{-k}}{\partial k_y} \frac{\partial \theta_{-k}}{\partial k_x} \right) \end{aligned} \quad (85)$$

where θ_k and ϕ_k are defined in Eq. (73). As a general result, we know that the symmetries of the Hamiltonian determine some properties of the Berry curvature. Effective time-reversal symmetry implies $\Omega(\mathbf{k}) = -\Omega(-\mathbf{k})$ (odd function), and inversion symmetry implies $\Omega(\mathbf{k}) = \Omega(-\mathbf{k})$ (even function). If both symmetries are present, we have $\Omega(\mathbf{k}) = 0$.

The Berry curvature is directly related to the transversal transport effects. It acts as an “artificial magnetic field” in momentum space, generating Hall-like transport. In the linear response theory, a magnetic field gradient can generate a spin current in the transverse direction, given by [22]:

$$j_y^{S,B} = \sigma_{xy} (-\partial_x B) \quad (86)$$

That is the spin Hall effect of magnons, and we call σ_{xy} the spin Hall conductivity. Also, the presence of a thermal gradient generates spin and heat currents, given by:

$$j_y^{S,T} = \alpha_{xy} (-\partial_x T) \quad (87)$$

$$j_y^{Q,T} = \kappa_{xy} (-\partial_x T) \quad (88)$$

These are the spin Nernst effect of magnons and the thermal Hall effect of magnons, respectively. The coefficient α_{xy} is called the spin Nernst coefficient, and κ_{xy} , the thermal Hall conductivity. The transport coefficients for a two-band antiferromagnet in the Néel state are given by [9, 22, 23, 104] (for the signs between the functions in the integrand, see [9]):

$$\sigma_{xy} = -\frac{1}{\hbar} \int_{BZ} \frac{d^2k}{(2\pi)^2} \left[n_k^\alpha \Omega_k^\alpha + n_k^\beta \Omega_k^\beta \right] \quad (89)$$

$$\alpha_{xy} = -\frac{k_B}{\hbar} \int_{BZ} \frac{d^2k}{(2\pi)^2} \left[c_1(n_k^\alpha) \Omega_k^\alpha - c_1(n_k^\beta) \Omega_k^\beta \right] \quad (90)$$

$$\kappa_{xy} = -\frac{k_B^2 T}{\hbar} \int_{BZ} \frac{d^2k}{(2\pi)^2} \left[c_2(n_k^\alpha) \Omega_k^\alpha + c_2(n_k^\beta) \Omega_k^\beta \right] \quad (91)$$

The functions $c_1(x)$ and $c_2(x)$ are defined as

$$c_1(x) = (1+x) \ln(1+x) - x \ln(x) \quad (92)$$

$$c_2(x) = (1+x) \left[\ln\left(\frac{1+x}{x}\right) \right]^2 - (\ln x)^2 - 2Li_2(-x). \quad (93)$$

Here, $Li_2(x)$ is Spence's dilogarithm function given by

$$Li_2(x) = \sum_{n=1}^{\infty} \frac{x^n}{n^2} \quad , \quad |x| \leq 1$$

$$Li_2(-x) = \frac{\pi^2}{16} - \frac{1}{2} (\ln x)^2 + \sum_{n=1}^{\infty} \frac{(-1)^{n-1}}{n^2 x^n} \quad , \quad x > 1 \quad (94)$$

We can predict the behavior of the transport coefficients for high temperatures noting that, for $k_B T \gg J_1$, the Bose-Einstein function can be approximated by $n_{\lambda,k} \approx k_B T / E_{\lambda,k}$. We also note that, when $x \rightarrow \infty$, the functions $c_i(x)$ behave as [25]:

$$c_1(x) = 1 + \ln(x)$$

$$c_2(x) = \frac{\pi^2}{3} - \frac{1}{x} \quad (95)$$

If $\Omega_k^\alpha = \pm \Omega_k^\beta$ and the Chern number of the bands is zero, we can show that

$$\sigma_{xy}(T \rightarrow \infty) = -\frac{k_B T}{\hbar^2} \int_{BZ} \frac{d^2k}{(2\pi)^2} \left(\frac{1}{\omega_k^\alpha} \pm \frac{1}{\omega_k^\beta} \right) \Omega_k^\alpha$$

$$\alpha_{xy}(T \rightarrow \infty) = \frac{k_B}{\hbar} \int_{BZ} \frac{d^2k}{(2\pi)^2} \left(\ln \omega_k^\alpha \mp \ln \omega_k^\beta \right) \Omega_k^\alpha$$

$$\kappa_{xy}(T \rightarrow \infty) = k_B \int_{BZ} \frac{d^2k}{(2\pi)^2} \left(\omega_k^\alpha \pm \omega_k^\beta \right) \Omega_k^\alpha \quad (96)$$

Appendix B shows that the Berry curvatures have the same sign for the Union Jack lattice and opposite signs for the brick-wall lattice, so the equations above are valid for both systems studied here. The results above show that in the high-temperature limit, α_{xy} and κ_{xy} are constants (asymptotic behavior), while σ_{xy} is proportional to T .

8 Brick-wall lattice

In the Union Jack lattice, all transport coefficients are non-null. Below, we will study a model that displays a magnonic equivalent of the QSHE, motivated by the fact that the prediction of this effect aroused a series of

theoretical generalizations under various physical contexts. First, we analyze the brick-wall lattice, which can be considered a distorted honeycomb lattice [105]. In this geometry, we consider the following Hamiltonian:

$$H = J_1 \sum_{\langle i,j \rangle} \mathbf{S}_i \cdot \mathbf{S}_j + J_2 \sum_{\langle i,j \rangle} \mathbf{S}_i \cdot \mathbf{S}_j + D \sum_{\langle\langle i,i' \rangle\rangle} \nu_{ii'} \hat{\mathbf{z}} \cdot \mathbf{S}_i \times \mathbf{S}_{i'} - A_1 \sum_i (S_i^z)^2 - A_2 \sum_j (S_j^z)^2 \quad (97)$$

where i denotes a site in sublattice A , and j in the sublattice B . As shown in Figure 10, we have exchange interactions J_1 and J_2 between sites A and B in a “wall of bricks” pattern. The arrows show the Dzyaloshinskii–Moriya interaction between sites AA and BB . We extend the model by considering different on-site anisotropies A_1 and A_2 . In an experimental setup, that can be brought about by placing the sample on a substrate or heterostructure, thereby producing a local environment of the atoms that differ for the two sublattices. In this case, the non-magnetic atoms (which are responsible for $A_1 \neq A_2 \neq 0$) break the effective time-reversal symmetry [106].

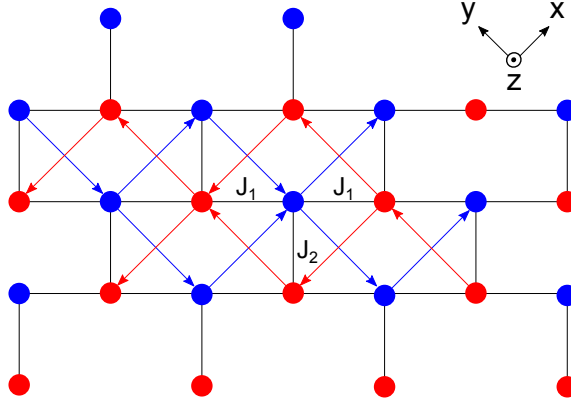


Figure 10: The AF brick-wall lattice described by Hamiltonian (97). The arrows represent DM interactions between NNN.

As before, we set the spacing of each sublattice equal to 1, and take the directions $\hat{\mathbf{x}}$ and $\hat{\mathbf{y}}$ along the diagonal axes of the two sublattices.

Following the same procedure as in the case of the Union Jack lattice, we get:

$$H_1 = \frac{(2+\alpha)}{2} J_1 S \sum_k \left[a_k^\dagger a_k + a_k a_k^\dagger + b_k^\dagger b_k + b_k b_k^\dagger \right] + \frac{3}{2} J_1 S \sum_k \left[\gamma_k^* (a_k b_{-k} + b_{-k} a_k) + \gamma_k (a_k^\dagger b_{-k}^\dagger + b_{-k}^\dagger a_k^\dagger) \right] \quad (98)$$

$$H_{SIA} = \frac{1}{2} (2S-1) \sum_k \left[A_1 (a_k^\dagger a_k + a_k a_k^\dagger) + A_2 (b_k^\dagger b_k + b_k b_k^\dagger) \right] \quad (99)$$

$$H_{DM} = 2SD \sum_k m_k \left[(a_k^\dagger a_k + a_k a_k^\dagger) - (b_k^\dagger b_k + b_k b_k^\dagger) \right] \quad (100)$$

where

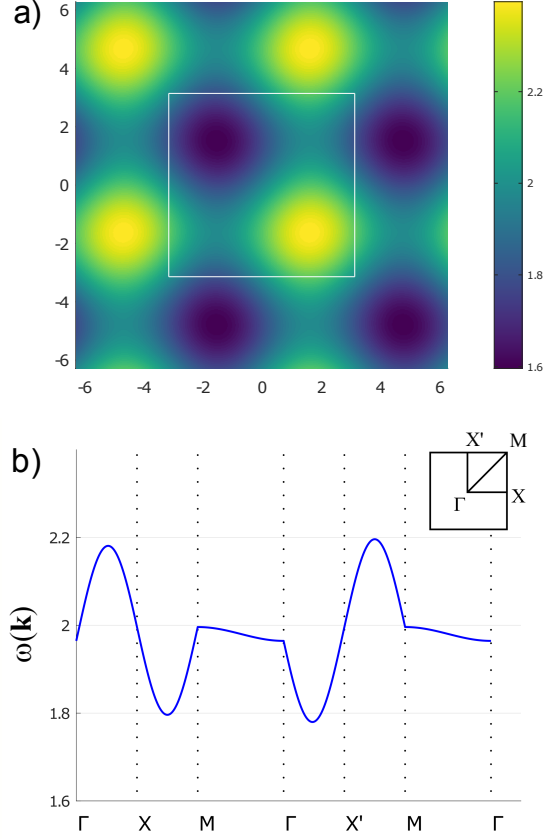


Figure 11: Degenerate energy bands of the AF brick-wall lattice (a) in the Brillouin zone (white square) and (b) between the high symmetry points. Theory parameters are $S = J_1 = A_1 = A_2 = \alpha = 1$, and $D = 0.2$. The bands are degenerate for $A_1 = A_2$.

$$\begin{aligned}
\alpha &= \frac{J_2}{J_1}, \quad \gamma_k = \delta_k + i\varepsilon_k \\
\delta_k &= \frac{1}{12} \left[(2 + \alpha) \cos\left(\frac{k_x}{2}\right) \cos\left(\frac{k_y}{2}\right) + \alpha \sin\left(\frac{k_x}{2}\right) \sin\left(\frac{k_y}{2}\right) \right], \\
\varepsilon_k &= -\frac{1}{12} \left[(2 - \alpha) \cos\left(\frac{k_x}{2}\right) \sin\left(\frac{k_y}{2}\right) + \alpha \sin\left(\frac{k_x}{2}\right) \cos\left(\frac{k_y}{2}\right) \right], \\
m_k &= \frac{1}{2} (\sin k_x - \sin k_y).
\end{aligned} \tag{101}$$

Note that $m_k = -m_{-k}$. We have now the Hamiltonian in Eq. (63) with parameters:

$$\begin{aligned}
r_{1k} &= \left(\frac{2+\alpha}{2} \right) J_1 S + 2SDm_k + \frac{1}{2} A_1 (2S-1) \\
r_{2k} &= \left(\frac{2+\alpha}{2} \right) J_1 S - 2SDm_k + \frac{1}{2} A_2 (2S-1) \\
h_{xk} &= \frac{3}{2} J_1 S \delta_k \\
h_{yk} &= -\frac{3}{2} J_1 S \varepsilon_k
\end{aligned} \tag{102}$$

The imaginary part of a Bogoliubov-de Gennes Hamiltonian is represented by h_{yk} (Eq. (64)). From the equations above, we see that $h_{yk} \propto \varepsilon_k = \text{Im}(\gamma_k)$. We also show in Appendix B that $h_{yk} \neq 0$ is a necessary condition for the Berry curvature to be non-zero. Hence, the complex lattice structure factor γ_k is responsible for the non-zero Berry curvature in this system.

Another feature of this system is that the Berry curvature is independent of the DMI. Retrieving the definitions $f \equiv h_x + ih_y$ and $w \equiv \sqrt{r^2 - |f|^2}$, from Eq. (B.15) we can see that the Berry curvature ultimately depends on h_x , h_y and r . As r is defined as $r \equiv (r_1 + r_2)/2$, from Eqs. (102) it is clear that neither h_x , h_y or r carry the DMI parameter (D cancels out in r). Hence, the Berry curvature does not depend on D . This result was also found for the AF honeycomb lattice [49, 68–70].

The energy spectrum of the system is given by Eqs. (76) with

$$\begin{aligned}
w(\mathbf{k}) &= \sqrt{r^2 - |f|^2} \\
\Delta(\mathbf{k}) &= \frac{1}{4} (A_1 - A_2) (2S-1) + 2SDm_k
\end{aligned} \tag{103}$$

Let us first consider the case $A_1 = A_2$. We have $\Delta(-\mathbf{k}) = -\Delta(\mathbf{k})$, which means $\omega_\beta(\mathbf{k}) = w(-\mathbf{k}) - \Delta(-\mathbf{k}) = w(\mathbf{k}) + \Delta(\mathbf{k}) = \omega_\alpha(\mathbf{k})$, and the bands are totally degenerate (Figure 11). This degeneracy is responsible for a pure spin Nernst effect of magnons, when a thermal gradient generates a transverse spin current without a net heat flow. This will be shown below.

Whereas the spin Hall and thermal Hall conductivities rely on ETRS breaking, the spin Nernst effect does not [70], and can exist even when the symmetry is present. Suppose the system shows ETRS. As we have seen, this implies $\Omega^\lambda(-\mathbf{k}) = -\Omega^\lambda(\mathbf{k})$. In Appendix B we show that, $\Omega^\beta(\mathbf{k}) = \Omega^\alpha(-\mathbf{k})$. These two properties imply $\Omega^\beta(\mathbf{k}) = -\Omega^\alpha(\mathbf{k})$, i.e., the bands have Berry curvatures of opposite sign. Degenerate bands with opposite Berry curvatures was also predicted for the honeycomb AF lattice in Ref. [69]. However, we note that in Ref. [70] it is mentioned that there is another basis convention that leads to non-degenerate bands and same-sign Berry curvatures. This does not impact the results in transport coefficients.

Considering the band degeneracy, the integrals in Eqs. (89) and (91) can be developed as:

$$\int d^2k \left[f(\omega_k^\alpha) \Omega_k^\alpha + f(\omega_k^\beta) \Omega_k^\beta \right] = \int d^2k \left[f(\omega_k^\alpha) - f(\omega_k^\beta) \right] \Omega_k^\alpha = 0 \tag{104}$$

The same does not occur for α_{xy} , as there is a subtraction in the integrand of Eq. (90), instead of a sum. Phenomenologically, that is the case presented in Section 2, where a thermal gradient $\partial_x T$ drives the two magnon modes in opposite transverse directions with the same intensity, making $\kappa_{xy} = 0$ and $\alpha_{xy} \neq 0$. That is a magnonic equivalent of the quantum spin Hall effect of electrons. We call that phenomenon a pure spin Nernst effect of magnons, when a temperature gradient generates a spin current without heat flow. A field gradient $\partial_x B$, on the other hand, drives the two magnon modes in the same direction with the same intensity, so the spin current vanishes, $\sigma_{xy} = 0$, while a heat current is present.

In the less strict case $A_1 \neq A_2$, the bands are not degenerate. Effective time-reversal symmetry is broken and all three transport coefficients can be non-null.

This brick-wall lattice is an example of the case discussed in Section 2 where the presence of an electric field (represented here by the DM term) is responsible for transverse transport of magnetic particles. This lattice has been proposed to describe the high-temperature superconductor $Ba_2CuO_{3+\delta}$ [107].

9 Results

9.1 Union Jack lattice

We now show the results of transversal transport for the antiferromagnetic Union Jack lattice, presented in Section 5. The results for energy dispersion for a variety of different parameters were already shown and discussed in the previous section. We set the parameters so that the Néel order is preserved, the Berry curvature is well-behaved, and the transport coefficients are non-null. The Berry curvature for typical parameters is represented in Figure 12. We see that the Berry curvature has the property $\Omega(\mathbf{k}) = \Omega(-\mathbf{k})$, which comes from the space inversion symmetry of the magnetic lattice (this symmetry also gives rise to the property $\omega_{\alpha,\beta}(\mathbf{k}) = \omega_{\alpha,\beta}(-\mathbf{k})$). For this system, ETRS is broken, but the Chern number is still zero:

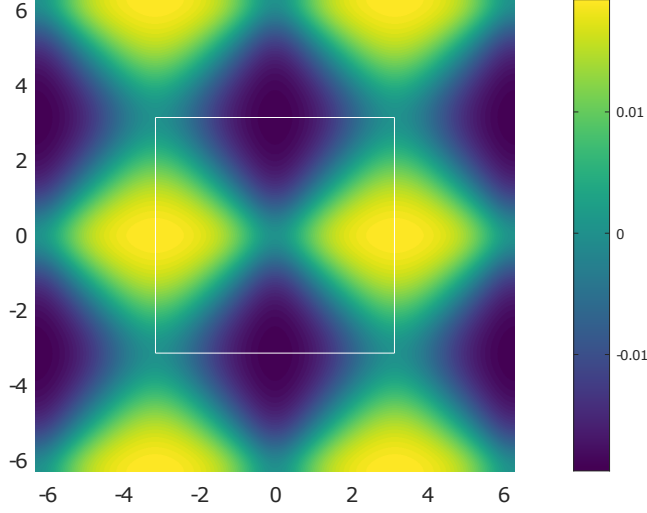


Figure 12: Berry curvature of AF Union Jack lattice magnon bands. Both bands have the same Berry curvature (see discussion in Appendix B). The parameters are $S = J_1 = A = 1$, $J_2 = D = 0.2$, and $\lambda = \alpha = 1.1$, which corresponds to the LSW bands in Figure 7 (solid red lines). The solid square is the Brillouin zone.

$$C_{\alpha,\beta} = \int \frac{d^2k}{2\pi} \Omega(\mathbf{k}) = 0 \quad (105)$$

That happens for every combination of Hamiltonian parameters, meaning the system is always topologically trivial and does not present protected edge states. That, however, does not necessarily mean the transport coefficients are null, as the integrands in Eqs. (89)-(91) are weighted by functions of the energies $f(\omega_{\alpha,\beta}(\mathbf{k}))$. The in-plane anisotropy $\alpha \neq 1$ generates an energetic imbalance between bands so that the integrals are found to be non-null. Although they are non-null, it is known that the transport coefficients for systems with $C = 0$ are much smaller compared to the cases where $C \neq 0$ [25].

To have a non-null Berry curvature, we need an imaginary term in the Hamiltonian ($h_y \neq 0$). As h_y comes from the DM interaction, we need $D \neq 0$: the DMI is crucial for a non-zero Berry curvature for the Union Jack lattice. That contrasts with systems where the DM interaction happens between sites of the same type (i. e., AA and BB) and contributes with a real term in the Hamiltonian, as it is the case of the honeycomb and brick-wall lattices. Also, we need $A \neq 0$ and $S \neq 1/2$ for non-zero energy in both bands gap, preventing the magnon occupation number (and the Berry curvature) from diverging when $T > 0$.

First, we present results for transport coefficients using the linear spin wave formalism (LSW). In all plots, we set $\hbar = k_B = 1$, so the units of the transport coefficients are the constants in front of the integrals in Eqs. (89-91). In Figure 13(a) we show the spin Hall conductivity σ_{xy} as a function of T for $S = J_1 = A = 1$, $J_2 = 0.2$, $\lambda = \alpha = 1.1$ and three values of D . At $T = 0$, σ_{xy} (and all other transport coefficients) vanishes due to the absence of magnon excitations. Magnons are thermally excited as the temperature increases, and the transport coefficients become finite. In Figures 13(b) and 13(c) we present the Nernst coefficient and

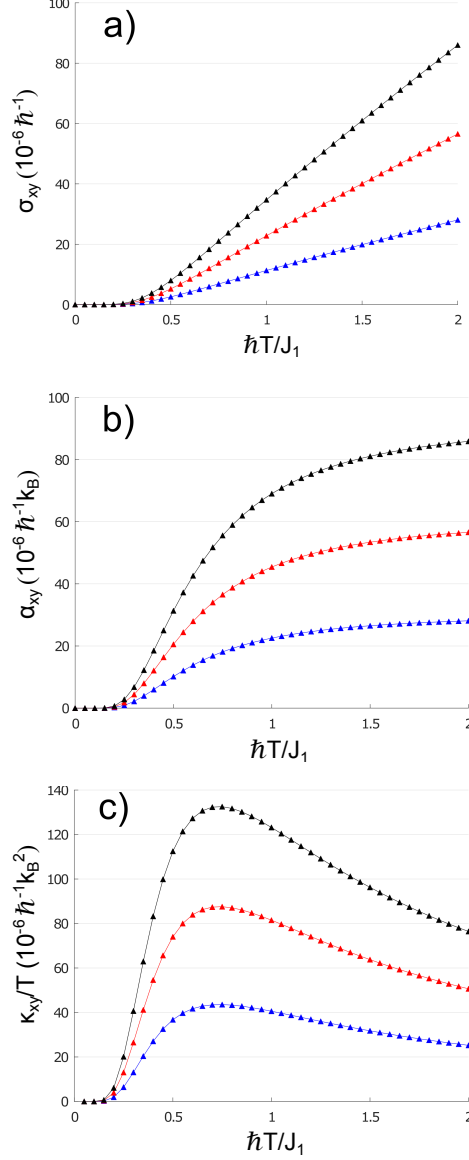


Figure 13: Transport coefficients of the AF Union Jack lattice for $D = 0.1$ (blue), $D = 0.2$ (red) and $D = 0.3$ (black). The other theory parameters are $S = J_1 = A = 1$, $J_2 = 0.2$, $\lambda = \alpha = 1.1$. (a) Spin Hall conductivity. (b) Spin Nernst coefficient. (c) Thermal Hall conductivity over T .

thermal Hall conductivity versus temperature for the same values of parameters. Focusing in the thermal Hall conductivity κ_{xy} versus T , the behavior of the curve resembles several other magnetic systems, like the FM and non-collinear AFM honeycomb lattice [48, 49], AFM checkerboard lattice [87], and FM kagome lattice, both in theoretical [72] and experimental [73] studies. For some systems, the sign of κ_{xy} can change with the choice of parameters (like in the Kitaev model [74]). In others, the curve κ_{xy} versus T can show peaks or valleys and even change sign with the temperature increase [40, 63]. This behavior was not observed in the AFM Union Jack lattice, where the curve κ_{xy} versus T is monotonic and asymptotic.

As we can see, all transport coefficients increase with D . If $J_2 = 0$ or $\alpha = 1$, a symmetry of the energy bands $\omega_{\alpha,\beta}(\mathbf{k})$ (namely, a rotation of the energy functions by 90°) makes all coefficients vanish identically. If $J_2 \neq 0$ and $\alpha \neq 1$, this symmetry is broken by an energetic inequivalence (mainly in the lower band, see Figure 5) of the axes k_x and k_y . That generates transverse transport. The effect of the off-plane exchange anisotropy λ is only quantitative: transverse transport exists even when $\lambda = 1$. Also, we can see that the high-temperature

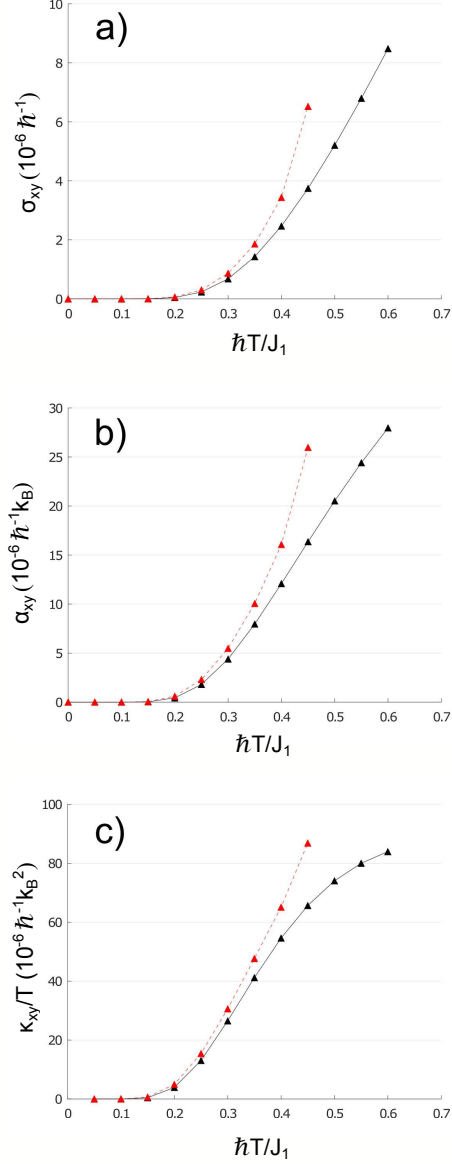


Figure 14: Effects of the MSW in the Union Jack lattice transport coefficients. (a) Spin Hall conductivity, (b) spin Nernst coefficient and (c) thermal Hall conductivity over T for the LSW (black) and MSW (dashed red) when anharmonic terms are included with a mean-field approach. The theory parameters are $S = J_1 = A = 1$, $J_2 = D = 0.2$, $\lambda = \alpha = 1.1$.

behavior of the coefficients is in accordance to Eqs. (96): α_{xy} and κ_{xy} have asymptotic behavior, while σ_{xy} is proportional to T .

Now, we consider the effect of anharmonic contributions using a modified spin wave theory, as mentioned in Section 5. In the linear spin wave treatment, the temperature dependence of the transport coefficients comes only from the Bose-Einstein distribution $n_k^{\alpha,\beta}$, the energy bands and Berry curvature being independent of temperature. In the self-consistent MSW theory, we partly include the effects of finite T and quantum fluctuations with a mean-field approach. We present the calculations in Appendix A. The corrections make the energy dispersion and Berry curvature temperature-dependent, correcting the transport coefficients for each temperature. In Figure 14 we present the results for MSW. The parameters are $S = J_1 = A = 1$, $J_2 = D = 0.2$, $\lambda = \alpha = 1.1$. The self-consistent corrections lower the energy bands (see Figure 8), raising the magnon population for a given temperature and increasing all transport coefficients. That happens until we reach a

temperature T_N (≈ 0.456 for the chosen parameters), where no self-consistent solution is found anymore. At this point, the magnetization vanishes (see Figure 9) signaling a transition to a disordered phase.

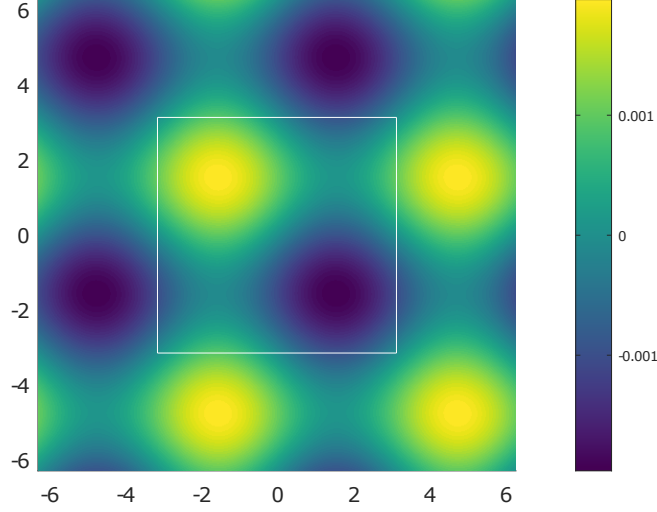


Figure 15: Berry curvature of band α for the AF brick-wall lattice (the band structure is shown in Figure 11). The parameters are $S = J_1 = A_1 = A_2 = \alpha = 1$ and $D = 0.2$. The band β has Berry curvature of opposite sign ($\Omega_\beta(\mathbf{k}) = -\Omega_\alpha(\mathbf{k})$), as discussed in Appendix B.

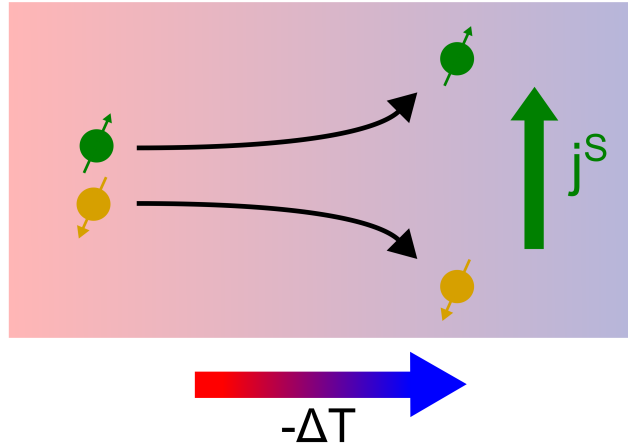


Figure 16: The pure spin Nernst effect of magnons, when different magnons are deflected on opposite directions with the same intensity, so it shows a spin current with no net heat flow.

9.2 Brick-wall lattice

We turn to the antiferromagnetic brick-wall lattice, firstly analyzing the case where $A_1 = A_2$, when the bands are degenerate. Without DMI ($D = 0$) the bands present even parity: $\omega_\beta(\mathbf{k}) = \omega_\alpha(\mathbf{k}) = \omega_\alpha(-\mathbf{k})$. The Hamiltonian $H = H_J + H_{SIA}$ is invariant under the effective time-reversal symmetry \mathcal{T}_{c_x} , as shown in Section 6. The presence of an ETRS results in an odd Berry curvature $\Omega(\mathbf{k}) = -\Omega(-\mathbf{k})$. Just like the case of the honeycomb lattice [69,70], a nonzero Berry curvature develops even without the DM interaction, but all transport coefficients are null. This non-zero Berry curvature also means that H_J must break the inversion symmetry. If we now introduce the DM interaction, the ETRS is broken in the Hamiltonian, but that does not affect the eigenstates.

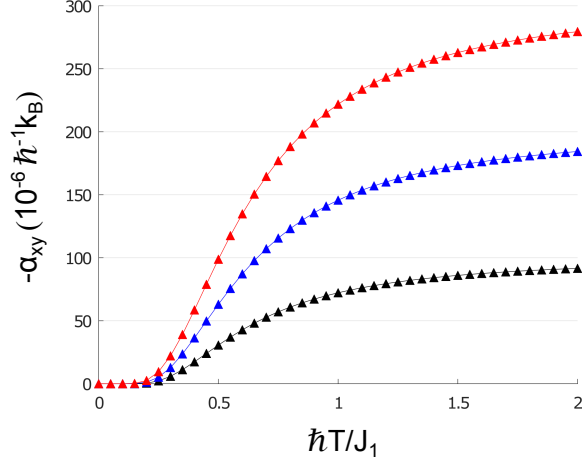


Figure 17: Spin Nernst coefficient as a function of temperature for the AF brick-wall lattice. The parameters are $S = J_1 = A_1 = A_2 = \alpha = 1$ and three different values of DM parameter: $D = 0.1$ (black), $D = 0.2$ (blue) and $D = 0.3$ (red). For $A_1 = A_2$, we have $\sigma_{xy} = \kappa_{xy} = 0$, and the system shows a pure spin Nernst effect of magnons.

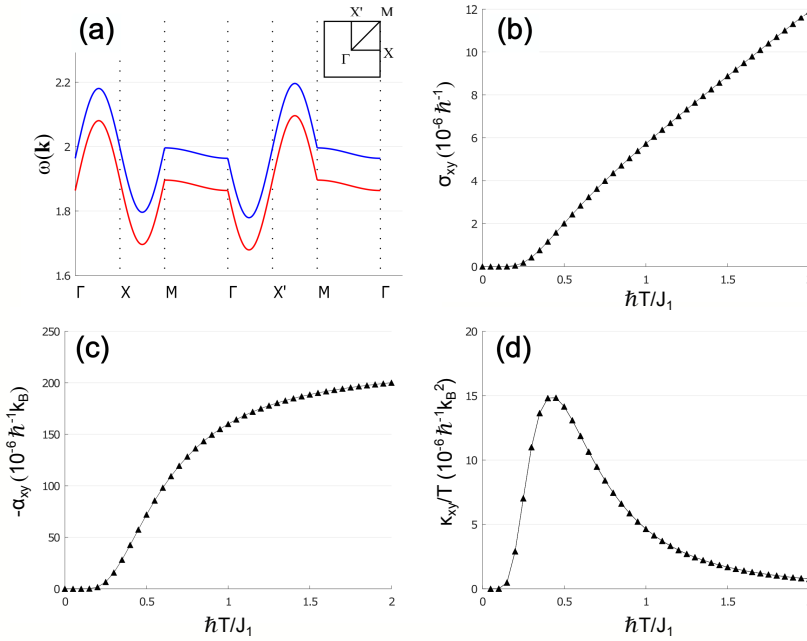


Figure 18: (a) Energy bands and (b-d) transport coefficients of the AF brick-wall lattice when $A_1 \neq A_2$. The parameters are $S = J_1 = \alpha = A_1 = 1$, $A_2 = 0.8$, and $D = 0.2$. All three coefficients are non-null.

The Berry curvature is unaffected and holds the odd parity (Figure 15). In a certain way, we can say that the ETRS is still present in the eigenstates of the system. As in the QSHE for electrons (mentioned in the Introduction), ETRS implies $C = 0$, and we have edge modes protected by the effective time-reversal symmetry. ETRS can protect gapped band topology and is associated with a two-valued or \mathbb{Z}_2 topological index [108]. For $D \neq 0$, we have $\sigma_{xy} = \kappa_{xy} = 0$ and $\alpha_{xy} \neq 0$, as discussed in Section 8. That happens even in the case of anisotropic exchange, when $\alpha = J_2/J_1 \neq 1$. The anisotropy α only changes quantitatively the spin Nernst coefficient.

In other words: when $A_1 = A_2$ and $D = 0$, the bands are totally degenerate and even, but $\Omega(\mathbf{k})$ is odd.

Thus, all transport coefficients vanish. A non-null D breaks the even parity of the bands. In the presence of a temperature gradient $\partial_x T$, the effect of the DM term is opposite for the two modes, driving the up/down magnons in opposite transverse directions with the same intensity. The transverse thermal current vanishes identically, but we have a net spin current ($\kappa_{xy} = 0$ and $\alpha_{xy} \neq 0$). This is the pure spin Nernst effect of magnons (Figure 16). When subjected to a magnetic field gradient $\partial_x B$, both magnon modes are driven to the same transverse direction with the same intensity, generating a heat current with no net spin current ($\sigma_{xy} = 0$).

The results for the spin Nernst coefficient as a function of temperature are shown in Figure 17. The parameters are $S = J_1 = A_1 = A_2 = \alpha = 1$, and three different values of D . We can see that α_{xy} increases with D , and has an asymptotic behavior in the high-temperature limit, as predicted.

All three transport coefficients are non-null for the general case $A_1 \neq A_2$. When subjected to a thermal gradient, up/down magnons are driven in opposite directions, but now with different intensities. The system shows non-null thermal and spin currents. The same can be said about the response to a magnetic field gradient, except now the magnons flow in the same direction. We show the results for this case in Figure 18.

10 Conclusions

In summary, we discussed magnon transport in antiferromagnetic topological insulators. We treated the antiferromagnetic Union Jack and the brick-wall lattices as examples, but the methods discussed here could be applied to several other lattices, such as the staggered and zig-zag square lattices [104].

Regarding the AF Union Jack lattice, we studied the band structure behavior for several parameters. The DMI generates a Berry curvature. It is an even function $\Omega(\mathbf{k}) = \Omega(-\mathbf{k})$ and identical for the two magnons. The bands are not degenerate, resulting in non-zero transport coefficients. Including magnon-magnon interactions with a mean-field approach lowers the energy bands, raising the thermal population. As a consequence, transverse transport is intensified.

Turning to the AF brick-wall lattice, the system presents degenerate bands with opposite Berry curvature. The Berry curvature is an odd function ($\Omega(\mathbf{k}) = -\Omega(-\mathbf{k})$), is independent of the DMI and relies on a complex structure factor. The system can present a pure spin Nernst effect, where $\alpha_{xy} \neq 0$ and $\sigma_{xy} = \kappa_{xy} = 0$. This effect is protected by an effective time-reversal symmetry, which can be broken by different single-ion anisotropies for the two sublattices. In this case the bands split, and all three transport coefficients are non-null.

We have shown that there is a fundamental difference in the microscopic origin of the spin Nernst effect on the two lattices. Although the Dzyaloshinskii-Moriya interaction (DMI) is an essential tool in both cases, it plays an entirely different role at the microscopic level. For example, the DMI induces a nonzero Berry curvature in the Union Jack lattice but not in the brick-wall lattice.

As far as we know, up to now, there are no real systems described by the Union Jack lattice. However, Wioland et al [109] found that lattices of hydrodynamically coupled bacterial vortices can spontaneously organize into distinct patterns characterized by ferro and antiferromagnetic order in a Union Jack lattice. They also found the existence of geometry-induced edge currents reminiscent of those in the quantum Hall effect. The Union Jack lattice could also be realized in optical lattices where synthetic DM interaction can be generated using laser beams [110]. In the next step, we intend to study the dynamics of the model following Refs. [111,112].

11 Acknowledgments

This work was supported by CAPES (Coordenação de Aperfeiçoamento de Pessoal de Nível Superior) and CNPq (Conselho Nacional de Desenvolvimento Científico e Tecnológico).

Appendix A Modified Spin Wave (MSW) approach

To calculate the effect of the lowest-order anharmonic contributions to the Union Jack lattice, presented in Section 5, we start with the Holstein-Primakoff transformation written up to four operator terms:

$$S_i^+ = \sqrt{2S} \left(a_i - \frac{a_i^\dagger a_i a_i}{4S} \right), \quad S_i^- = \sqrt{2S} \left(a_i^\dagger - \frac{a_i^\dagger a_i^\dagger a_i}{4S} \right), \quad S_i^z = S - a_i^\dagger a_i \quad (\text{A.1})$$

on a sublattice A and

$$S_j^+ = \sqrt{2S} \left(b_j^\dagger - \frac{b_j^\dagger b_j^\dagger b_j}{4S} \right), \quad S_j^- = \sqrt{2S} \left(b_j - \frac{b_j^\dagger b_j b_j^\dagger}{4S} \right), \quad S_j^z = -S + b_j^\dagger b_j \quad (\text{A.2})$$

on sublattice B . Taking (A.1) and (A.2) into Hamiltonian (51) we find, neglecting all constant terms:

$$H = H_1 + H_2 + H_{DM} + H_{SIA} \quad (\text{A.3})$$

where

$$H_1 = J_1 S \sum_{\langle i,j \rangle} \left(a_i^\dagger a_i + b_j^\dagger b_j + a_i b_j + a_i^\dagger b_j^\dagger \right) + \frac{J_1}{4} \sum_{\langle i,j \rangle} \left(a_i b_j^\dagger b_j b_j + a_i^\dagger a_i a_i b_j + a_i^\dagger b_j^\dagger b_j^\dagger b_j + a_i^\dagger a_i^\dagger a_i b_j^\dagger + 4a_i^\dagger a_i b_j^\dagger b_j \right) \quad (\text{A.4})$$

$$H_2 = S \sum_{\langle\langle i,j \rangle\rangle} J_{2,ij} \left[a_i a_j^\dagger + a_i^\dagger a_j - \lambda \left(a_i^\dagger a_i + a_j^\dagger a_j \right) \right] + \frac{1}{4} \sum_{\langle\langle i,j \rangle\rangle} J_{2,ij} \left(a_i a_j^\dagger a_j^\dagger a_j + a_i^\dagger a_i a_i a_j^\dagger + a_i^\dagger a_j^\dagger a_j a_j + a_i^\dagger a_i^\dagger a_i a_j - 4\lambda a_i^\dagger a_i a_j^\dagger a_j \right) \quad (\text{A.5})$$

$$H_{DM} = iDS \sum_{\langle i,j \rangle} \nu_{ij} \left(a_i b_j - a_i^\dagger b_j^\dagger \right) + i \frac{D}{4} \sum_{\langle i,j \rangle} \nu_{ij} \left(-a_i b_j^\dagger b_j b_j - a_i^\dagger a_i a_i b_j + a_i^\dagger b_j^\dagger b_j^\dagger b_j + a_i^\dagger a_i^\dagger a_i b_j^\dagger \right) \quad (\text{A.6})$$

$$H_{SIA} = 2AS \left(\sum_{i \in A} a_i^\dagger a_i + \sum_{j \in B} b_j^\dagger b_j \right) - A \left(\sum_{i \in A} a_i^\dagger a_i a_i^\dagger a_i + \sum_{j \in B} b_j^\dagger b_j b_j^\dagger b_j \right) \\ = A(2S - 1) \left(\sum_{i \in A} a_i^\dagger a_i + \sum_{j \in B} b_j^\dagger b_j \right) - A \left(\sum_{i \in A} a_i^\dagger a_i^\dagger a_i a_i + \sum_{j \in B} b_j^\dagger b_j^\dagger b_j b_j \right) \quad (\text{A.7})$$

where, in the SIA term, we have used $a_i^\dagger a_i a_i^\dagger a_i = a_i^\dagger a_i + a_i^\dagger a_i^\dagger a_i a_i$ (and similarly for the b_j operators) to normal order the quartic terms.

Considering only the quadratic terms on the expressions above, we obtain the linear spin wave theory (LSW) exposed in the main text. We include the quartic terms to consider the interactions between magnons and perform a mean-field decoupling to obtain an effective quadratic Hamiltonian (modified spin theory, MSW). We use the well-known relation between quantum operators (ignoring the zeroth-order terms $\langle AB \rangle \langle CD \rangle$ which only add a global constant energy to the spectrum):

$$ABCD = \langle AB \rangle CD + AB \langle CD \rangle + \langle AC \rangle BD + AC \langle BD \rangle + \langle AD \rangle BC + AD \langle BC \rangle \quad (\text{A.8})$$

The only non-null mean-field terms are $\langle a_i^\dagger a_j \rangle$, $\langle b_i^\dagger b_j \rangle$, $\langle a_i b_j \rangle$, $\langle b_i a_j \rangle$ and their complex conjugates (see discussion in the end of this Appendix). For instance, the first quartic term in H_1 decouples as:

$$a_i b_j^\dagger b_j b_j = 2 \langle b_j^\dagger b_j \rangle a_i b_j + 2 \langle a_i b_j \rangle b_j^\dagger b_j \quad (\text{A.9})$$

We rename the mean-field terms as

$$g_1 = \langle a_i^\dagger a_i \rangle, \quad g_2 = \langle b_j^\dagger b_j \rangle, \quad g_3 = \langle a_i b_j \rangle, \\ g_4 = \langle a_i^\dagger b_j^\dagger \rangle, \quad g_5 = \langle a_i^\dagger a_j \rangle, \quad g_6 = \langle a_i a_j^\dagger \rangle \quad (\text{A.10})$$

Noting that g_3 and g_4 can be complex, we can also write:

$$\begin{aligned} g_3 &= G_1 + iG_2, & g_4 &= G_1 - iG_2, \\ \rightarrow g_3 + g_4 &= 2G_1, & g_3 - g_4 &= 2iG_2 \end{aligned} \quad (\text{A.11})$$

With these definitions, we write

$$\begin{aligned} H_1 &= J_1 S \sum_{\langle i,j \rangle} \left(a_i^\dagger a_i + b_j^\dagger b_j + a_i b_j + a_i^\dagger b_j^\dagger \right) - J_1 \sum_{\langle i,j \rangle} \left[(g_2 + G_1) a_i^\dagger a_i + (g_1 + G_1) b_j^\dagger b_j + \right. \\ &\quad \left. + \left(\frac{g_1 + g_2}{2} + G_1 \right) (a_i b_j + a_i^\dagger b_j^\dagger) - iG_2 (a_i b_j - a_i^\dagger b_j^\dagger) \right] \end{aligned} \quad (\text{A.12})$$

$$H_2 = S \sum_{\langle\langle i,j \rangle\rangle} J_{2,ij} \left[a_i a_j^\dagger + a_i^\dagger a_j - \lambda (a_i^\dagger a_i + a_j^\dagger a_j) \right] - \sum_{\langle\langle i,j \rangle\rangle} J_{2,ij} \left[\left(\frac{g_5 + g_6}{2} - \lambda g_1 \right) (a_i^\dagger a_i + a_j^\dagger a_j) + \right. \quad (\text{A.13})$$

$$\left. + g_1 (a_i^\dagger a_j + a_i a_j^\dagger) - \lambda (g_6 a_i^\dagger a_j + g_5 a_i a_j^\dagger) \right] \quad (\text{A.14})$$

$$H_{DM} = iDS \sum_{\langle i,j \rangle} \nu_{ij} (a_i b_j - a_i^\dagger b_j^\dagger) + D \sum_{\langle i,j \rangle} \nu_{ij} \left[G_2 (a_i^\dagger a_i + b_j^\dagger b_j) - \frac{i}{2} (g_1 + g_2) (a_i b_j - a_i^\dagger b_j^\dagger) \right]$$

$$H_{SIA} = A(2S - 1) \left(\sum_{i \in A} a_i^\dagger a_i + \sum_{j \in B} b_j^\dagger b_j \right) - 4A \left(\sum_{i \in A} g_1 a_i^\dagger a_i + \sum_{j \in B} g_2 b_j^\dagger b_j \right) \quad (\text{A.15})$$

Evaluating:

$$H_1 + H_{DM} = \sum_{\langle i,j \rangle} \left\{ [J_1 (S - g_2 - G_1) + \nu_{ij} D G_2] a_i^\dagger a_i + [J_1 (S - g_1 - G_1) + \nu_{ij} D G_2] b_j^\dagger b_j + \right. \quad (\text{A.16})$$

$$\left. + J_1 \left(S - \frac{g_1 + g_2}{2} - G_1 \right) (a_i b_j + a_i^\dagger b_j^\dagger) + i \left[J_1 G_2 + \nu_{ij} D \left(S - \frac{g_1 + g_2}{2} \right) \right] (a_i b_j - a_i^\dagger b_j^\dagger) \right\}$$

$$H_2 = \sum_{\langle\langle i,j \rangle\rangle} J_{2,ij} \left[\left(-\frac{g_5 + g_6}{2} - \lambda (S - g_1) \right) (a_i^\dagger a_i + a_j^\dagger a_j) + \right. \quad (\text{A.17})$$

$$\left. + (S - g_1) (a_i^\dagger a_j + a_i a_j^\dagger) + \lambda (g_6 a_i^\dagger a_j + g_5 a_i a_j^\dagger) \right]$$

$$H_{SIA} = A[(2S - 1) - 4g_1] \sum_{i \in A} a_i^\dagger a_i + A[(2S - 1) - 4g_2] \sum_{j \in B} b_j^\dagger b_j \quad (\text{A.18})$$

Let Γ_i be new parameters defined as:

$$\begin{aligned} \Gamma_1 &= S - \left(\frac{g_1 + g_2}{2} + G_1 \right) \\ \Gamma_2 &= (S - G_1 - g_2) \\ \Gamma_3 &= (S - G_1 - g_1) \\ \Gamma_4 &= S - \frac{g_1 + g_2}{2} \\ \Gamma_5 &= -\frac{g_5 + g_6}{2} - \lambda (S - g_1) \\ \Gamma_6 &= (2S - 1) - 4g_1 \\ \Gamma_7 &= (2S - 1) - 4g_2 \end{aligned} \quad (\text{A.19})$$

We can rewrite the Hamiltonian in terms of eight temperature-dependent parameters: Γ_i and G_2 (not all linearly independent). Fourier transforming and symmetrizing the operators, we get:

$$\begin{aligned} H_1 + H_{DM} = & 2 \sum_k \left[(J_1 \Gamma_2 + m_k D G_2) \left(a_k^\dagger a_k + a_k a_k^\dagger \right) + (J_1 \Gamma_3 + m_k D G_2) \left(b_k^\dagger b_k + b_k b_k^\dagger \right) + \right. \\ & + \gamma_k J_1 \Gamma_1 \left(a_k b_{-k} + b_{-k} a_k + a_k^\dagger b_{-k}^\dagger + b_{-k}^\dagger a_k^\dagger \right) + \\ & \left. + i (\gamma_k J_1 G_2 + m_k D \Gamma_4) \left(a_k b_{-k} + b_{-k} a_k - a_k^\dagger b_{-k}^\dagger - b_{-k}^\dagger a_k^\dagger \right) \right] \end{aligned} \quad (\text{A.20})$$

$$H_2 = J_2 \sum_k \left\{ \Gamma_5 [(\alpha + 1) - 2\lambda \eta_k] + 2\eta_k (1 - \lambda^2) (\Gamma_3 + \Gamma_4 - \Gamma_1) \right\} \left(a_k^\dagger a_k + a_k a_k^\dagger \right) \quad (\text{A.21})$$

$$H_{SIA} = \frac{A}{2} \sum_k \left[\Gamma_6 \left(a_k^\dagger a_k + a_k a_k^\dagger \right) + \Gamma_7 \left(b_k^\dagger b_k + b_k b_k^\dagger \right) \right] \quad (\text{A.22})$$

We have, then, a renormalized Hamiltonian matrix

$$H_k = \begin{pmatrix} M_k & 0 \\ 0 & M_{-k}^* \end{pmatrix}, \quad M_k = \begin{pmatrix} r_1 & f^* \\ f & r_2 \end{pmatrix} \quad (\text{A.23})$$

with temperature-dependent parameters:

$$\begin{aligned} r_1^{(MSW)} &= 2 (J_1 \Gamma_2 + m_k D G_2) + J_2 \left\{ \Gamma_5 [(\alpha + 1) - 2\lambda \eta_k] + 2\eta_k (1 - \lambda^2) (\Gamma_3 + \Gamma_4 - \Gamma_1) \right\} + \frac{A}{2} \Gamma_6 \\ r_2^{(MSW)} &= 2 (J_1 \Gamma_3 + m_k D G_2) + \frac{A}{2} \Gamma_7 \\ h_x^{(MSW)} &= 2 \gamma_k J_1 \Gamma_1 \\ h_y^{(MSW)} &= 2 (\gamma_k J_1 G_2 + m_k D \Gamma_4) \end{aligned} \quad (\text{A.24})$$

To obtain temperature-dependent expressions for the mean-field parameters Γ_i (or equivalently, g_i), we Fourier transform the thermal averages $\langle a_i^\dagger a_j \rangle$, $\langle b_i^\dagger b_j \rangle$, $\langle a_i b_j \rangle$ and $\langle b_i a_j \rangle$, and make a change of basis using

$$\psi_k = T_k \varphi_k \quad (\text{A.25})$$

with $\psi_k^\dagger = (a_k^\dagger \ b_{-k} \ a_{-k} \ b_k^\dagger)$ being the original basis, and $\varphi_k^\dagger = (\alpha_k^\dagger \ \beta_{-k} \ \alpha_{-k} \ \beta_k^\dagger)$ being a new basis. The matrix T_k is given by Eq. (75). As mentioned before, in a particle-hole Hamiltonian, the Hilbert space is duplicated, so we can find an irreducible 2×2 representation for the transformation above:

$$\begin{pmatrix} a_k \\ b_{-k}^\dagger \end{pmatrix} = \begin{pmatrix} u^* & -v \\ -v^* & u \end{pmatrix} \begin{pmatrix} \alpha_k \\ \beta_{-k}^\dagger \end{pmatrix} \quad (\text{A.26})$$

The thermal averages, after a change of basis, can be written in terms of the parameters u and v and the occupation number of the bands $n_k^{\alpha, \beta}$. For instance:

$$\begin{aligned} \langle a_i^\dagger a_i \rangle &= \frac{2}{N} \sum_k \langle a_k^\dagger a_k \rangle = \frac{2}{N} \sum_k \left[|u|^2 n_k^\alpha + |v|^2 (1 + n_k^\beta) \right] \\ \langle b_i^\dagger b_i \rangle &= \frac{2}{N} \sum_k \langle b_k^\dagger b_k \rangle = \frac{2}{N} \sum_k \left[|v|^2 (1 + n_k^\alpha) + |u|^2 n_k^\beta \right] \end{aligned} \quad (\text{A.27})$$

where N is the total number of sites. Here,

$$\begin{aligned} n_k^\alpha &= \langle \alpha_k^\dagger \alpha_k \rangle = \left[\exp(E_k^\beta / k_B T) - 1 \right]^{-1} \\ n_k^\beta &= \langle \beta_k^\dagger \beta_k \rangle = \left[\exp(E_k^\alpha / k_B T) - 1 \right]^{-1} \end{aligned} \quad (\text{A.28})$$

are the Bose-Einstein distributions. The terms $\langle \alpha_k^\dagger \alpha_k \rangle$ and $\langle \beta_k^\dagger \beta_k \rangle$ are the only thermal averages in the new basis that are not zero. To illustrate that, let's consider a term of the form

$$\langle \alpha_k \beta_{-k} \rangle = \frac{1}{Z} \sum_n e^{-\beta E_k^n} \langle n | \alpha_k \beta_{-k} | n \rangle \quad (\text{A.29})$$

The matrix element $\langle n | \alpha_k \beta_{-k} | n \rangle$ is an overlap of the state $\beta_{-k} | n \rangle$ and $\alpha_k^\dagger | n \rangle$. Both states are eigenstates of H_k , but as they do not have identical sets of occupation numbers of α and β bosons, their overlap is zero. Hence $\langle \alpha_k \beta_{-k} \rangle$ and its complex conjugate are zero. This occurs for every other thermal average, except $\langle \alpha_k^\dagger \alpha_k \rangle$ and $\langle \beta_k^\dagger \beta_k \rangle$.

Performing the procedure detailed above, we obtain temperature-dependent expressions for the g_i and G_i parameters:

$$\begin{aligned} g_1 &= \frac{2}{N} \sum_k \left[|u|^2 n_k^\alpha + |v|^2 (1 + n_k^\beta) \right] \\ g_2 &= \frac{2}{N} \sum_k \left[|u|^2 n_k^\beta + |v|^2 (1 + n_k^\alpha) \right] \\ g_5 &= \frac{2}{N} \sum_k \eta_k \left[|u|^2 n_k^\alpha + |v|^2 (1 + n_k^\beta) \right] \\ g_6 &= \frac{2}{N} \sum_k \eta_k \left[|u|^2 (1 + n_k^\alpha) + |v|^2 n_k^\beta \right] \\ G_1 &= -\frac{2}{N} \sum_k \gamma_k x v (1 + n_k^\alpha + n_k^\beta) \\ G_2 &= \frac{2}{N} \sum_k \gamma_k y v (1 + n_k^\alpha + n_k^\beta) \end{aligned} \quad (\text{A.30})$$

where we defined $u = x + iy$. The sublattice (staggered) magnetization is given by

$$m = S - \langle a_i^\dagger a_i \rangle = S - \frac{2}{N} \sum_k \left[|u|^2 n_k^\alpha + |v|^2 (1 + n_k^\beta) \right] \quad (\text{A.31})$$

The temperature dependence comes from the Bose-Einstein factors. In the continuum limit, the summation becomes an integral over the Brillouin zone:

$$\frac{2}{N} \sum_{\mathbf{k}} [\clubsuit] \rightarrow \int_{BZ} \frac{d^2 k}{(2\pi)^2} [\clubsuit] \quad (\text{A.32})$$

For each temperature, we can obtain the Γ_i factors self-consistently from the Eqs. (A.30) and Eqs. (A.19). These terms renormalize the Hamiltonian.

In summary, the effective Hamiltonian becomes temperature-dependent when we include quartic terms through a mean-field decoupling. For each temperature, coefficients Γ_i that renormalize the Hamiltonian parameters can be obtained self-consistently through (A.19) and (A.30). All the equations in Section 5 remain the same, but with the renormalized parameters r_1 , r_2 and f , following Eqs. (A.24).

Appendix B Berry curvature of a Bogoliubov-de Gennes Hamiltonian

We start with the Berry curvature given by Eq. (48) [25]:

$$\Omega_{xy}^n(\mathbf{k}) = i \sum_{\mu\nu} \varepsilon_{\mu\nu} \left[\eta \frac{\partial T_k^\dagger}{\partial k_\mu} \eta \frac{\partial T_k}{\partial k_\nu} \right]_{nn} \quad (\text{B.1})$$

The matrices η and T_k are block diagonal:

$$\eta = \begin{pmatrix} 1 & 0 & 0 & 0 \\ 0 & -1 & 0 & 0 \\ 0 & 0 & -1 & 0 \\ 0 & 0 & 0 & 1 \end{pmatrix} = \begin{pmatrix} \sigma_z & 0 \\ 0 & -\sigma_z \end{pmatrix} \quad (\text{B.2})$$

$$T_k = \begin{pmatrix} u_k^* & -v_k & 0 & 0 \\ -v_k^* & u_k & 0 & 0 \\ 0 & 0 & u_{-k} & -v_{-k}^* \\ 0 & 0 & -v_{-k} & u_{-k}^* \end{pmatrix} = \begin{pmatrix} T_\alpha & 0 \\ 0 & T_\beta \end{pmatrix}, \quad (\text{B.3})$$

so we can perform a block multiplication:

$$\eta \frac{\partial T_k^\dagger}{\partial k_\mu} \eta \frac{\partial T_k}{\partial k_\nu} = \begin{pmatrix} \sigma_z \frac{\partial T_\alpha^\dagger}{\partial k_\mu} \sigma_z \frac{\partial T_\alpha}{\partial k_\nu} & 0 \\ 0 & \sigma_z \frac{\partial T_\beta^\dagger}{\partial k_\mu} \sigma_z \frac{\partial T_\beta}{\partial k_\nu} \end{pmatrix} \quad (\text{B.4})$$

The expression for the Berry curvature can be reduced to 2×2 representation

$$\Omega_{xy}^{(n)}(\mathbf{k}) = i \sum_{\mu\nu} \varepsilon_{\mu\nu} \left(\sigma_z \frac{\partial T_{\alpha,\beta}^\dagger}{\partial k_\mu} \sigma_z \frac{\partial T_{\alpha,\beta}}{\partial k_\nu} \right)_{nn} \quad (\text{B.5})$$

where we can choose the α or β sector. We focus on the particle states, remembering that for the α -sector, it corresponds to the first column of T_α ($n = 1$), and for the β -sector, to the second column of T_β ($n = 2$).

Focusing on the α -sector first, we have:

$$\Omega_{xy}^\alpha(\mathbf{k}) = i \sum_{\mu\nu} \varepsilon_{\mu\nu} \left(\sigma_z \frac{\partial T_\alpha^\dagger}{\partial k_\mu} \sigma_z \frac{\partial T_\alpha}{\partial k_\nu} \right)_{11} \quad (\text{B.6})$$

Using $T_\alpha = \begin{pmatrix} u_k^* & -v_k \\ -v_k^* & u_k \end{pmatrix}$ (see Section 5), we have (we suppress the index k for clearer notation):

$$\begin{aligned} \sigma_z \frac{\partial T_\alpha^\dagger}{\partial k_x} \sigma_z \frac{\partial T_\alpha}{\partial k_y} &= \begin{pmatrix} \frac{\partial u}{\partial k_x} & -\frac{\partial v}{\partial k_x} \\ \frac{\partial v^*}{\partial k_x} & -\frac{\partial u^*}{\partial k_x} \end{pmatrix} \begin{pmatrix} \frac{\partial u^*}{\partial k_y} & -\frac{\partial v}{\partial k_y} \\ \frac{\partial v}{\partial k_y} & -\frac{\partial u}{\partial k_y} \end{pmatrix} \\ \rightarrow \left[\sigma_z \frac{\partial T_\alpha^\dagger}{\partial k_x} \sigma_z \frac{\partial T_\alpha}{\partial k_y} \right]_{11} &= \frac{\partial u}{\partial k_x} \frac{\partial u^*}{\partial k_y} - \frac{\partial v}{\partial k_x} \frac{\partial v^*}{\partial k_y} \end{aligned} \quad (\text{B.7})$$

and we can write

$$\begin{aligned} \sum_{\mu\nu} \varepsilon_{\mu\nu} \left(\sigma_z \frac{\partial T_\alpha^\dagger}{\partial k_\mu} \sigma_z \frac{\partial T_\alpha}{\partial k_\nu} \right)_{11} &= \left(\frac{\partial u}{\partial k_x} \frac{\partial u^*}{\partial k_y} - \frac{\partial v}{\partial k_x} \frac{\partial v^*}{\partial k_y} \right) - \left(\frac{\partial u}{\partial k_y} \frac{\partial u^*}{\partial k_x} - \frac{\partial v}{\partial k_y} \frac{\partial v^*}{\partial k_x} \right) \\ &= \left(\frac{\partial u}{\partial k_x} \frac{\partial u^*}{\partial k_y} - \frac{\partial v}{\partial k_x} \frac{\partial v^*}{\partial k_y} \right) - C.C. \end{aligned} \quad (\text{B.8})$$

The expression for the Berry curvature of the particle α state reduces to

$$\begin{aligned} \Omega_{xy}^\alpha(\mathbf{k}) &= i \left[\left(\frac{\partial u}{\partial k_x} \frac{\partial u^*}{\partial k_y} - \frac{\partial v}{\partial k_x} \frac{\partial v^*}{\partial k_y} \right) - C.C. \right] = i \left[2i \operatorname{Im} \left(\frac{\partial u}{\partial k_x} \frac{\partial u^*}{\partial k_y} - \frac{\partial v}{\partial k_x} \frac{\partial v^*}{\partial k_y} \right) \right] \\ \Omega_{xy}^\alpha(\mathbf{k}) &= -2 \operatorname{Im} \left(\frac{\partial u}{\partial k_x} \frac{\partial u^*}{\partial k_y} - \frac{\partial v}{\partial k_x} \frac{\partial v^*}{\partial k_y} \right) \end{aligned} \quad (\text{B.9})$$

Using $u = e^{i\phi} \cosh\left(\frac{\theta}{2}\right)$ and $v = \left(\frac{r-w}{2w}\right)^{1/2}$ we get $\operatorname{Im} \frac{\partial v}{\partial k_x} \frac{\partial v^*}{\partial k_y} = 0$ because v is real):

$$\begin{aligned}\frac{\partial u}{\partial k_x} &= e^{i\phi} \left[i \cosh \frac{\theta}{2} \left(\frac{\partial \phi}{\partial k_x} \right) + \frac{1}{2} \sinh \frac{\theta}{2} \left(\frac{\partial \theta}{\partial k_x} \right) \right] \\ \frac{\partial u^*}{\partial k_y} &= e^{-i\phi} \left[-i \cosh \frac{\theta}{2} \left(\frac{\partial \phi}{\partial k_y} \right) + \frac{1}{2} \sinh \frac{\theta}{2} \left(\frac{\partial \theta}{\partial k_y} \right) \right]\end{aligned}\quad (\text{B.10})$$

and using $\sinh\left(\frac{\theta}{2}\right) \cosh\left(\frac{\theta}{2}\right) = \frac{1}{2} \sinh \theta$ we finally get

$$\Omega_{xy}^\alpha(\mathbf{k}) = -\frac{1}{2} \sinh \theta_k \left(\frac{\partial \phi_k}{\partial k_x} \frac{\partial \theta_k}{\partial k_y} - \frac{\partial \phi_k}{\partial k_y} \frac{\partial \theta_k}{\partial k_x} \right) \quad (\text{B.11})$$

For the β -sector, the initial expression is

$$\Omega_{xy}^\beta(\mathbf{k}) = i \sum_{\mu\nu} \varepsilon_{\mu\nu} \left(\sigma_z \frac{\partial T_\beta^\dagger}{\partial k_\mu} \sigma_z \frac{\partial T_\beta}{\partial k_\nu} \right)_{22} \quad (\text{B.12})$$

And noting that $T_\beta(\mathbf{k}) = T_\alpha^*(-\mathbf{k})$, it is easy to show that

$$\Omega_{xy}^\beta(\mathbf{k}) = -\frac{1}{2} \sinh \theta_{-k} \left(\frac{\partial \phi_{-k}}{\partial k_x} \frac{\partial \theta_{-k}}{\partial k_y} - \frac{\partial \phi_{-k}}{\partial k_y} \frac{\partial \theta_{-k}}{\partial k_x} \right) \quad (\text{B.13})$$

The general relation between the Berry curvatures of the two bands is $\Omega_{xy}^\beta(\mathbf{k}) = \Omega_{xy}^\alpha(-\mathbf{k})$. When these are even functions ($\Omega_{xy}^\alpha(\mathbf{k}) = \Omega_{xy}^\alpha(-\mathbf{k})$, as it is the case of the Union Jack lattice), both Berry curvatures have the same sign: $\Omega_{xy}^\beta(\mathbf{k}) = \Omega_{xy}^\alpha(\mathbf{k})$. But when they are odd functions ($\Omega_{xy}^\alpha(\mathbf{k}) = -\Omega_{xy}^\alpha(-\mathbf{k})$, as it is the case of the brick-wall lattice) the Berry curvatures have opposite signs: $\Omega_{xy}^\beta(\mathbf{k}) = -\Omega_{xy}^\alpha(\mathbf{k})$.

It is possible to show that the hole-states, which correspond to the second and third columns of T_k , have opposite Berry curvature in the same band index as a consequence of particle-hole symmetry:

$$\begin{aligned}\Omega_{xy}^{\alpha(hole)}(\mathbf{k}) &= -\Omega_{xy}^{\alpha(particle)}(\mathbf{k}) \\ \Omega_{xy}^{\beta(hole)}(\mathbf{k}) &= -\Omega_{xy}^{\beta(particle)}(\mathbf{k})\end{aligned}\quad (\text{B.14})$$

Evaluating Eq. (B.11) with the definitions in Section 4, we arrive at the expression:

$$\begin{aligned}\Omega_{xy}^\alpha(\mathbf{k}) &= -\frac{1}{2} \frac{1}{w^3 |f|} \left\{ \left(h_x \frac{\partial h_y}{\partial k_x} - h_y \frac{\partial h_x}{\partial k_x} \right) \left[\frac{r}{|f|} \left(h_x \frac{\partial h_x}{\partial k_y} + h_y \frac{\partial h_y}{\partial k_y} \right) - |f| \frac{\partial r}{\partial k_y} \right] \right. \\ &\quad \left. - \left(h_x \frac{\partial h_y}{\partial k_y} - h_y \frac{\partial h_x}{\partial k_y} \right) \left[\frac{r}{|f|} \left(h_x \frac{\partial h_x}{\partial k_x} + h_y \frac{\partial h_y}{\partial k_x} \right) - |f| \frac{\partial r}{\partial k_x} \right] \right\}\end{aligned}\quad (\text{B.15})$$

and from this we can plot the Berry curvature of any system, knowing the Hamiltonian parameters h_x , h_y and r . We stress here that the imaginary part of the Hamiltonian comes from h_y . From the expression above, we see it is crucial that $h_y \neq 0$ for a non-null Berry curvature. In other words: an imaginary term in the Hamiltonian is necessary for the system to have a non-null Berry curvature.

References

- [1] D. J. Thouless, M. Kohmoto, M. P. Nightingale, and M. den Nijs, “Quantized hall conductance in a two-dimensional periodic potential,” *Phys. Rev. Lett.*, vol. 49, pp. 405–408, Aug. 1982.
- [2] F. D. M. Haldane, “Model for a quantum Hall effect without Landau levels: Condensed-matter realization of the “parity anomaly”,” *Phys. Rev. Lett.*, vol. 61, pp. 2015–2018, Oct. 1988.
- [3] C. L. Kane and E. J. Mele, “ Z_2 topological order and the quantum spin Hall effect,” *Phys. Rev. Lett.*, vol. 95, Sept. 2005.
- [4] P. Phillips, *Advanced solid state physics*. Cambridge, England: Cambridge University Press, 2 ed., Mar. 2012.
- [5] A. S. Teixeira Pires, *A brief introduction to topology and differential geometry in condensed matter physics*. IOP Concise Physics, San Rafael, CA: Morgan & Claypool, Mar. 2019.
- [6] D. Ghader, “Insights on magnon topology and valley-polarization in 2d bilayer quantum magnets,” *New J. Phys.*, vol. 23, p. 053022, May 2021.
- [7] K. Nakata, S. K. Kim, J. Klinovaja, and D. Loss, “Magnonic topological insulators in antiferromagnets,” *Phys. Rev. B*, vol. 96, p. 224414, Dec. 2017.
- [8] Y. Liu, J. Li, and Q. Liu, “Antiferromagnetic Chern insulators (preprint),” 2022.
- [9] K. Nakata and S. K. Kim, “Topological Hall effects of magnons in ferrimagnets,” *J. Phys. Soc. Jpn.*, vol. 90, p. 081004, Aug. 2021.
- [10] V. Bonbien, F. Zhuo, A. Salimath, O. Ly, A. Abbout, and A. Manchon, “Topological aspects of antiferromagnets,” *J. Phys. D: Appl. Phys.*, vol. 55, p. 103002, Nov. 2021.
- [11] Y. Zhang, S. Okamoto, and D. Xiao, “Spin-Nernst effect in the paramagnetic regime of an antiferromagnetic insulator,” *Phys. Rev. B*, vol. 98, July 2018.
- [12] B. Li, S. Sandhoefner, and A. A. Kovalev, “Intrinsic spin Nernst effect of magnons in a noncollinear antiferromagnet,” *Phys. Rev. Res.*, vol. 2, p. 013079, Jan 2020.
- [13] K.-S. Kim, K. H. Lee, S. B. Chung, and J.-G. Park, “Magnon topology and thermal hall effect in trimerized triangular lattice antiferromagnet,” *Phys. Rev. B*, vol. 100, Aug. 2019.
- [14] D. Bhowmick and P. Sengupta, “Topological magnon bands in the flux state of shastry-sutherland lattice model,” *Phys. Rev. B*, vol. 101, June 2020.
- [15] J. Romhányi, K. Penc, and R. Ganesh, “Hall effect of triplons in a dimerized quantum magnet,” *Nat. Commun.*, vol. 6, Apr. 2015.
- [16] P. A. McClarty, F. Krüger, T. Guidi, S. F. Parker, K. Refson, A. W. Parker, D. Prabhakaran, and R. Coldea, “Topological triplon modes and bound states in a Shastry-Sutherland magnet,” *Nat. Phys.*, vol. 13, pp. 736–741, May 2017.
- [17] D. Bhowmick and P. Sengupta, “Weyl triplons in,” *Phys. Rev. B*, vol. 104, Aug. 2021.
- [18] S. A. Owerre, “Floquet topological magnons,” *J. Phys. Commun.*, vol. 1, p. 021002, Sept. 2017.
- [19] L. Smejkal, R. Gonzalez-Hernandez, T. Jungwirth, and J. Sinova, “Crystal time-reversal symmetry breaking and spontaneous Hall effect in collinear antiferromagnets,” *Sci. Adv.*, vol. 6, June 2020.
- [20] H. Kondo, Y. Akagi, and H. Katsura, “Non-hermiticity and topological invariants of magnon Bogoliubov-de Gennes systems,” *Prog. Theor. Exp. Phys.*, vol. 2020, p. 12A104, Oct. 2020.
- [21] J. H. Han, J.-H. Park, and P. A. Lee, “Consideration of thermal Hall effect in undoped cuprates,” *Phys. Rev. B*, vol. 99, p. 205157, May 2019.

- [22] J. H. Han and H. Lee, “Spin chirality and Hall-like transport phenomena of spin excitations,” *J. Phys. Soc. Jpn.*, vol. 86, no. 1, p. 011007, 2017.
- [23] R. Matsumoto, R. Shindou, and S. Murakami, “Thermal Hall effect of magnons in magnets with dipolar interaction,” *Phys. Rev. B*, vol. 89, p. 054420, 2014.
- [24] A. A. Kovalev and V. Zyuzin, “Spin torque and Nernst effects in Dzyaloshinskii-Moriya ferromagnets,” *Phys. Rev. B*, vol. 93, p. 161106, 2016.
- [25] R. Samajdar, S. Chatterjee, S. Sachdev, and M. S. Scheurer, “Thermal Hall effect in square-lattice spin liquids: A Schwinger boson mean-field study,” *Phys. Rev. B*, vol. 99, p. 165126, Apr. 2019.
- [26] S. Park, N. Nagaosa, and B.-J. Yang, “Thermal Hall effect, spin Nernst effect, and spin density induced by a thermal gradient in collinear ferrimagnets from magnon-phonon interaction,” *Nano Lett.*, vol. 20, pp. 2741–2746, Feb. 2020.
- [27] X. S. Wang and X. R. Wang, “Topological magnonics,” *J. Appl. Phys.*, vol. 129, p. 151101, Apr. 2021.
- [28] R. Shindou, R. Matsumoto, S. Murakami, and J. Ohe, “Topological chiral magnonic edge mode in a magnonic crystal,” *Phys. Rev. B*, vol. 87, p. 174427, May 2013.
- [29] L. Zhang, J. Ren, J.-S. Wang, and B. Li, “Topological magnon insulator in insulating ferromagnet,” *Phys. Rev. B*, vol. 87, p. 144101, Apr. 2013.
- [30] L. Zhang, J. Ren, J.-S. Wang, and B. Li, “Topological nature of the phonon Hall effect,” *Phys. Rev. Lett.*, vol. 105, p. 225901, Nov. 2010.
- [31] M. Kawano and C. Hotta, “Thermal Hall effect and topological edge states in a square-lattice antiferromagnet,” *Phys. Rev. B*, vol. 99, p. 054422, feb 2019.
- [32] A. Mook, J. Henk, and I. Mertig, “Tunable magnon Weyl points in ferromagnetic pyrochlores,” *Phys. Rev. Lett.*, vol. 117, p. 157204, Oct 2016.
- [33] R. Shindou, J. Ohe, R. Matsumoto, S. Murakami, and E. Saitoh, “Chiral spin-wave edge modes in dipolar magnetic thin films,” *Phys. Rev. B*, vol. 87, p. 174402, May 2013.
- [34] H. Lee, J. H. Han, and P. A. Lee, “Thermal Hall effect of spins in a paramagnet,” *Phys. Rev. B*, vol. 91, p. 125413, Mar 2015.
- [35] F.-Y. Li, Y.-D. Li, Y. B. Kim, L. Balents, Y. Yu, and G. Chen, “Weyl magnons in breathing pyrochlore antiferromagnets,” *Nat. Commun.*, vol. 7, p. 12691, Sept. 2016.
- [36] Y. He, J. Moore, and C. M. Varma, “Berry phase and anomalous Hall effect in a three-orbital tight-binding hamiltonian,” *Phys. Rev. B*, vol. 85, p. 155106, Apr 2012.
- [37] A. V. Chumak, V. I. Vasyuchka, A. A. Serga, and B. Hillebrands, “Magnon spintronics,” *Nat. Phys.*, vol. 11, pp. 453–461, June 2015.
- [38] H. Katsura, N. Nagaosa, and P. A. Lee, “Theory of the thermal Hall effect in quantum magnets,” *Phys. Rev. Lett.*, vol. 104, p. 066403, Feb 2010.
- [39] Y. Onose, T. Ideue, H. Katsura, Y. Shiomi, N. Nagaosa, and Y. Tokura, “Observation of the magnon Hall effect,” *Science*, vol. 329, pp. 297–299, July 2010.
- [40] A. Mook, J. Henk, and I. Mertig, “Magnon Hall effect and topology in kagome lattices: A theoretical investigation,” *Phys. Rev. B*, vol. 89, p. 134409, Apr 2014.
- [41] R. Matsumoto and S. Murakami, “Theoretical prediction of a rotating magnon wave packet in ferromagnets,” *Phys. Rev. Lett.*, vol. 106, no. 19, p. 197202, 2011.
- [42] S. K. Kim, H. Ochoa, R. Zarzuela, and Y. Tserkovnyak, “Realization of the Haldane-Kane-Mele model in a system of localized spins,” *Phys. Rev. Lett.*, vol. 117, no. 22, p. 227201, 2016.

- [43] S. S. Pershoguba, S. Banerjee, J. C. Lashley, J. Park, H. Ågren, G. Aeppli, and A. V. Balatsky, “Dirac magnons in honeycomb ferromagnets,” *Phys. Rev. X*, vol. 8, p. 011010, Jan 2018.
- [44] L. Chen, J.-H. Chung, B. Gao, T. Chen, M. B. Stone, A. I. Kolesnikov, Q. Huang, and P. Dai, “Topological spin excitations in honeycomb ferromagnet CrI_3 ,” *Phys. Rev. X*, vol. 8, p. 041028, Nov 2018.
- [45] J. Fransson, A. M. Black-Schaffer, and A. V. Balatsky, “Magnon Dirac materials,” *Phys. Rev. B*, vol. 94, p. 075401, Aug 2016.
- [46] S. A. Owerre, “A first theoretical realization of honeycomb topological magnon insulator,” *J. Phys.: Condens. Matter*, vol. 28, no. 38, p. 386001, 2016.
- [47] S. A. Owerre and J. Nsofini, “Squeezed Dirac and topological magnons in a bosonic honeycomb optical lattice,” *J. Phys.: Condens. Matter*, vol. 29, p. 455802, Oct. 2017.
- [48] S. A. Owerre, “Topological honeycomb magnon Hall effect: A calculation of thermal Hall conductivity of magnetic spin excitations,” *J. Appl. Phys.*, vol. 120, p. 043903, July 2016.
- [49] S. A. Owerre, “Noncollinear antiferromagnetic Haldane magnon insulator,” *J. Appl. Phys.*, vol. 121, p. 223904, June 2017.
- [50] S. A. Owerre, “Dirac magnon nodal loops in quasi-2d quantum magnets,” *Sci. Rep.*, vol. 7, p. 6931, July 2017.
- [51] S. A. Owerre, “Magnon Hall effect in ab-stacked bilayer honeycomb quantum magnets,” *Phys. Rev. B*, vol. 94, p. 094405, Sep 2016.
- [52] S. A. Owerre, “Topological thermal Hall effect in frustrated kagome antiferromagnets,” *Phys. Rev. B*, vol. 95, p. 014422, Jan 2017.
- [53] S. A. Owerre, “Weyl magnons in noncoplanar stacked kagome antiferromagnets,” *Phys. Rev. B*, vol. 97, p. 094412, Mar 2018.
- [54] X. S. Wang, Y. Su, and X. R. Wang, “Topologically protected unidirectional edge spin waves and beam splitter,” *Phys. Rev. B*, vol. 95, p. 014435, Jan 2017.
- [55] P. A. Pantaleón and Y. Xian, “Edge states in a ferromagnetic honeycomb lattice with armchair boundaries,” *Physica B*, vol. 530, pp. 191–194, Feb. 2018.
- [56] R. Chisnell, J. S. Helton, D. E. Freedman, D. K. Singh, R. I. Bewley, D. G. Nocera, and Y. S. Lee, “Topological magnon bands in a kagome lattice ferromagnet,” *Phys. Rev. Lett.*, vol. 115, p. 147201, Sep 2015.
- [57] Y. Su and X. R. Wang, “Chiral anomaly of Weyl magnons in stacked honeycomb ferromagnets,” *Phys. Rev. B*, vol. 96, p. 104437, Sep 2017.
- [58] R. Seshadri and D. Sen, “Topological magnons in a kagome-lattice spin system with xxz and Dzyaloshinskii-Moriya interactions,” *Phys. Rev. B*, vol. 97, p. 134411, Apr 2018.
- [59] A. Mook, J. Henk, and I. Mertig, “Magnon waveguide with nanoscale confinement constructed from topological magnon insulators,” *Phys. Rev. B*, vol. 91, p. 174409, May 2015.
- [60] M. Hirschberger, R. Chisnell, Y. S. Lee, and N. P. Ong, “Thermal Hall effect of spin excitations in a kagome magnet,” *Phys. Rev. Lett.*, vol. 115, p. 106603, Sep 2015.
- [61] A. Mook, J. Henk, and I. Mertig, “Spin dynamics simulations of topological magnon insulators: From transverse current correlation functions to the family of magnon Hall effects,” *Phys. Rev. B*, vol. 94, p. 174444, Nov 2016.
- [62] Y. Su, X. S. Wang, and X. R. Wang, “Magnonic Weyl semimetal and chiral anomaly in pyrochlore ferromagnets,” *Phys. Rev. B*, vol. 95, p. 224403, Jun 2017.

- [63] X. Cao, K. Chen, and D. He, “Magnon Hall effect on the lieb lattice,” *J. Phys.: Condens. Matter*, vol. 27, no. 16, p. 166003, 2015.
- [64] G. Wirth, M. Ölschläger, and A. Hemmerich, “Evidence for orbital superfluidity in the p-band of a bipartite optical square lattice,” *Nat. Phys.*, vol. 7, pp. 147–153, Dec. 2010.
- [65] P. S. Kumar, I. F. Herbut, and R. Ganesh, “Dirac hamiltonians for bosonic spectra,” *Phys. Rev. Res.*, vol. 2, p. 033035, Jul 2020.
- [66] W. Li, D. N. Sheng, C. S. Ting, and Y. Chen, “Fractional quantum spin Hall effect in flat-band checker-board lattice model,” *Phys. Rev. B*, vol. 90, p. 081102, Aug 2014.
- [67] S. M. Rezende, R. L. Rodríguez-Suárez, and A. Azevedo, “Diffusive magnonic spin transport in antiferromagnetic insulators,” *Phys. Rev. B*, vol. 93, p. 054412, Feb 2016.
- [68] R. Cheng, S. Okamoto, and D. Xiao, “Spin Nernst effect of magnons in collinear antiferromagnets,” *Phys. Rev. Lett.*, vol. 117, no. 21, p. 217202, 2016.
- [69] V. A. Zyuzin and A. A. Kovalev, “Magnon spin Nernst effect in antiferromagnets,” *Phys. Rev. Lett.*, vol. 117, p. 217203, Nov 2016.
- [70] H. Zhang and R. Cheng, “A perspective on magnon spin Nernst effect in antiferromagnets,” *Appl. Phys. Lett.*, vol. 120, p. 090502, Feb. 2022.
- [71] Y. Lu, X. Guo, V. Koval, and C. Jia, “Topological thermal Hall effect driven by spin-chirality fluctuations in frustrated antiferromagnets,” *Phys. Rev. B*, vol. 99, p. 054409, Feb 2019.
- [72] P. Laurell and G. A. Fiete, “Magnon thermal Hall effect in kagome antiferromagnets with Dzyaloshinskii-Moriya interactions,” *Phys. Rev. B*, vol. 98, p. 094419, Sep 2018.
- [73] H. Doki, M. Akazawa, H.-Y. Lee, J. H. Han, K. Sugii, M. Shimozawa, N. Kawashima, M. Oda, H. Yoshida, and M. Yamashita, “Spin thermal hall conductivity of a kagome antiferromagnet,” *Phys. Rev. Lett.*, vol. 121, Aug. 2018.
- [74] K. Li, “Thermal Hall conductivity with sign change in the Heisenberg–Kitaev kagome magnet,” *Commun. Theor. Phys.*, vol. 75, p. 015702, Dec. 2022.
- [75] A. Mook, J. Henk, and I. Mertig, “Thermal Hall effect in noncollinear coplanar insulating antiferromagnets,” *Phys. Rev. B*, vol. 99, p. 014427, Jan 2019.
- [76] M. Hirschberger, J. W. Krizan, R. J. Cava, and N. P. Ong, “Large thermal Hall conductivity of neutral spin excitations in a frustrated quantum magnet,” *Science*, vol. 348, pp. 106–109, Apr. 2015.
- [77] V. Baltz, A. Manchon, M. Tsoi, T. Moriyama, T. Ono, and Y. Tserkovnyak, “Antiferromagnetic spintronics,” *Rev. Mod. Phys.*, vol. 90, p. 015005, Feb 2018.
- [78] T. Jungwirth, J. Sinova, A. Manchon, X. Marti, J. Wunderlich, and C. Felser, “The multiple directions of antiferromagnetic spintronics,” *Nat. Phys.*, vol. 14, pp. 200–203, Mar. 2018.
- [79] R. A. Duine, K.-J. Lee, S. S. P. Parkin, and M. D. Stiles, “Synthetic antiferromagnetic spintronics,” *Nat. Phys.*, vol. 14, pp. 217–219, Mar. 2018.
- [80] O. Gomonay, V. Baltz, A. Brataas, and Y. Tserkovnyak, “Antiferromagnetic spin textures and dynamics,” *Nat. Phys.*, vol. 14, pp. 213–216, Mar. 2018.
- [81] J. Zelezny, P. Wadley, K. Olejnik, A. Hoffmann, and H. Ohno, “Spin transport and spin torque in antiferromagnetic devices,” *Nat. Phys.*, vol. 14, pp. 220–228, Mar. 2018.
- [82] P. Nemec, M. Fiebig, T. Kampfrath, and A. V. Kimel, “Antiferromagnetic opto-spintronics,” *Nat. Phys.*, vol. 14, pp. 229–241, Mar. 2018.
- [83] L. Smejkal, Y. Mokrousov, B. Yan, and A. H. MacDonald, “Topological antiferromagnetic spintronics,” *Nat. Phys.*, vol. 14, pp. 242–251, Mar. 2018.

- [84] M. B. Jungfleisch, W. Zhang, and A. Hoffmann, “Perspectives of antiferromagnetic spintronics,” *Phys. Lett. A*, vol. 382, pp. 865–871, Apr. 2018.
- [85] H. Chen, Q. Niu, and A. H. MacDonald, “Anomalous Hall effect arising from noncollinear antiferromagnetism,” *Phys. Rev. Lett.*, vol. 112, p. 017205, Jan 2014.
- [86] J. Kübler and C. Felser, “Non-collinear antiferromagnets and the anomalous Hall effect,” *Europhys. Lett.*, vol. 108, p. 67001, Dec. 2014.
- [87] A. S. T. Pires, “Topological magnons in the antiferromagnetic checkerboard lattice,” *Physica E*, vol. 118, p. 113899, Apr. 2020.
- [88] A. S. T. Pires, “Dynamical spin conductivity of the Heisenberg antiferromagnetic checkerboard lattice,” *Braz. J. Phys.*, vol. 51, pp. 429–433, Apr. 2021.
- [89] P. Le and M. Yarmohammadi, “Magnonic heat transport in the Lieb lattice,” *J. Magn. Magn. Mater.*, vol. 469, pp. 623–628, Jan. 2019.
- [90] P. G. de Oliveira and A. S. T. Pires, “Transversal transport of magnons in a modified Lieb lattice,” *Physica B*, vol. 654, p. 414721, Apr. 2023.
- [91] A. Bhattacharya and B. Pal, “Flat bands and nontrivial topological properties in an extended Lieb lattice,” *Phys. Rev. B*, vol. 100, Dec. 2019.
- [92] Y. Aharonov and A. Casher, “Topological quantum effects for neutral particles,” *Phys. Rev. Lett.*, vol. 53, pp. 319–321, Jul 1984.
- [93] G. D. Mahan, *Many-particle physics*. Physics of Solids and Liquids, New York, NY: Springer, 2 ed., Dec. 2012.
- [94] D. Malz, J. Knolle, and A. Nunnenkamp, “Topological magnon amplification,” *Nat. Commun.*, vol. 10, Sept. 2019.
- [95] D. Bhowmick, H. Sun, B. Yang, and P. Sengupta, “Tuning bulk topological magnon properties with light-induced magnons,” *Phys. Rev. B*, vol. 107, June 2023.
- [96] R. Kubo, M. Toda, and N. Hashitsume, *Statistical physics II*. Springer Series in Solid-State Sciences, Berlin, Germany: Springer, 1985 ed., June 1985.
- [97] A. S. T. Pires, *Theoretical tools for spin models in magnetic systems*. 2053-2563, IOP Publishing, 2021.
- [98] J. Colpa, “Diagonalization of the quadratic boson hamiltonian,” *Physica A*, vol. 93, pp. 327–353, Sept. 1978.
- [99] H. Katsura, N. Nagaosa, and A. V. Balatsky, “Spin current and magnetoelectric effect in noncollinear magnets,” *Phys. Rev. Lett.*, vol. 95, p. 057205, Jul 2005.
- [100] A. Collins, J. McEvoy, D. Robinson, C. J. Hamer, and Z. Weihong, “Quantum spin model with frustration on the Union Jack lattice,” *Phys. Rev. B*, vol. 73, p. 024407, Jan 2006.
- [101] R. F. Bishop, P. H. Y. Li, D. J. J. Farnell, and C. E. Campbell, “Magnetic order on a frustrated spin-1/2 Heisenberg antiferromagnet on the Union Jack lattice,” *Phys. Rev. B*, vol. 82, p. 024416, Jul 2010.
- [102] W. Zheng, J. Oitmaa, and C. J. Hamer, “Phase diagram of the frustrated Heisenberg antiferromagnet on the Union Jack lattice,” *Phys. Rev. B*, vol. 75, p. 184418, May 2007.
- [103] R. F. Bishop and P. H. Y. Li, “A frustrated quantum spin-s model on the Union Jack lattice with spins $s > 1/2$,” *Eur. Phys. J. B*, vol. 81, pp. 37–48, Apr. 2011.
- [104] H. Kondo and Y. Akagi, “Nonlinear magnon spin Nernst effect in antiferromagnets and strain-tunable pure spin current,” *Phys. Rev. Res.*, vol. 4, p. 013186, Mar 2022.

- [105] J.-M. Hou and W. Chen, “Hidden symmetry and protection of Dirac points on the honeycomb lattice,” *Sci. Rep.*, vol. 5, p. 17571, Dec. 2015.
- [106] R. Hidalgo-Sacoto, R. I. Gonzalez, E. E. Vogel, S. Allende, J. D. Mella, C. Cardenas, R. E. Troncoso, and F. Munoz, “Magnon valley Hall effect in CrI_3 -based van der Waals heterostructures,” *Phys. Rev. B*, vol. 101, p. 205425, May 2020.
- [107] Z. Wang, S. Zhou, W. Chen, and F.-C. Zhang, “ $t - j$ model on the effective brick-wall lattice for the recently discovered high-temperature superconductor $Ba_2CuO_{3+\delta}$,” *Phys. Rev. B*, vol. 101, p. 180509, May 2020.
- [108] H. Kondo, Y. Akagi, and H. Katsura, “ \mathbb{Z}_2 topological invariant for magnon spin Hall systems,” *Phys. Rev. B*, vol. 99, p. 041110(R), Jan. 2019.
- [109] H. Wioiland, F. G. Woodhouse, J. Dunkel, and R. E. Goldstein, “Ferromagnetic and antiferromagnetic order in bacterial vortex lattices,” *Nat. Phys.*, vol. 12, pp. 341–345, Jan. 2016.
- [110] M. Olschlager, G. Wirth, T. Kock, and A. Hemmerich, “Topologically induced avoided band crossing in an optical checkerboard lattice,” *Phys. Rev. Lett.*, vol. 108, p. 075302, Feb 2012.
- [111] F. Azizi and H. Rezaia, “Spin transport properties of anisotropic Heisenberg antiferromagnet on honeycomb lattice in the presence of magnetic field,” *Eur. Phys. J. B*, vol. 93, Feb. 2020.
- [112] F. Azizi and H. Rezaia, “Dynamical and static spin structure factors of Heisenberg antiferromagnet on honeycomb lattice in the presence of Dzyaloshinskii-Moriya interaction (preprint),” 2021.